Remote Sensing of Environment 139 (2013) 149–170

Contents lists available at ScienceDirect

Remote Sensing of Environment

journal homepage: www.elsevier.com/locate/rse

Radiative transfer modeling in the Earth–Atmosphere system with DART model

Eloi Grau *, Jean-Philippe Gastellu-Etchegorry [1]

Centre d'Etudes Spatiales de la BIOsphère (CESBIO), CNES, CNRS, IRD, UPS, 18 Av. E.Belin, 31401 Toulouse, France

ARTICLE INFO

Article history:
Received 12 December 2011
Received in revised form 1 July 2013
Accepted 2 July 2013
Available online 4 September 2013

Keywords:
3D radiative transfer model
Earth atmosphere radiative coupling
Optical remote sensing images simulation

ABSTRACT

The atmosphere strongly affects satellite measurements of Earth surfaces in the optical domain. Modeling this influence is complex. This is typically the case of the "Earth–Atmosphere" radiative coupling in the presence of Earth surfaces with spatially variable optical properties. In that case, it may be very difficult to couple Earth and cloud-free atmosphere radiative transfer models. This explains why an atmosphere module was input into the Earth radiative transfer (R.T.) model DART (Discrete Anisotropic Radiative Transfer) in order to simulate accurately satellite images of natural and urban Earth surfaces. This paper presents how DART simulates the atmosphere R.T. in the short wave and thermal infrared domains. The atmosphere is divided into 3 zones: bottom atmosphere (BA), mid atmosphere (MA) and high atmosphere (HA). The 3D distribution is arbitrary in BA and horizontally constant with any vertical distribution in MA and HA. The "Earth–Atmosphere" R.T. is modeled in 5 stages. 1) Atmosphere R.T. (i.e., atmosphere thermal emission and/or sun radiation scattering). 2) Earth surface R.T. (i.e., Earth thermal emission and/or atmosphere and direct sun radiation scattering). 3) Atmosphere R.T. (i.e., Earth radiation scattering). 4) Earth surface R.T. (i.e., scattering of downward atmosphere radiation). 5) Simulation of satellite reflectance and/or brightness temperature images. The approach takes into account the earth curvature and the atmosphere non-Beer law behavior in the presence of strongly varying spectral properties. It uses optimally located scattering points for improving atmosphere R.T. accuracy, and it reduces computer time through the use of pre-computed transfer functions that transfer radiation between the different atmosphere levels (BA, MA, HA). Moreover, it can simulate automatically an atmosphere geometry that optimizes the trade-off "Computer time–Accuracy" of simulations. The robustness and accuracy of the DART atmosphere modeling were successfully validated with theoretical cases and with the MODTRAN atmosphere R.T. model.

1. Introduction

Modeling the radiative regime in the "Earth–Atmosphere" system is more and more a prerequisite for studying natural and urban surfaces, using bi-directional reflectance (BRDF) and directional brightness temperature (BTDF) distribution functions (Laurent et al., 2011). This is especially true in the optical domain, from the visible up to the thermal infrared domain. Indeed, in these spectral domains, the order of magnitude of atmosphere signals can be equal or larger than that of land surface signals that arise at the top of the atmosphere (TOA). Thus, the simulation of accurate TOA signals requires an accurate modeling of radiative transfer (R.T.) at 3 levels. 1) Earth surface, with taking into account the 3D heterogeneity of Earth surfaces. 2) Atmosphere, with taking into account the vertical distribution of gasses and aerosols. 3) Radiative coupling of the "Earth–Atmosphere" system.

Different methods are used to solve the atmosphere R.T. A few examples are given here: the discrete-ordinate (DISORT—Stamnes, Tsay, Wiscombe, & Laszlo, 2000), the invariant embedding method (Adams and Kattawar, 1970), the adding and doubling method (Hansen, 1971), the matrix operator method (Plass, Kattawar, & Catchings, 1973), the spherical harmonics method (Zhai, Kattawar, & Yang, 2008), the multi-component method (Zege et al., 1993), the spherical harmonics discrete ordinate method (Evans, 1998), the F_N method (Garcia and Siewert, 1989), the Successive Order of Scattering (SOS)method (Lenoble et al., 2007), and the Monte Carlo method (Deutschmann et al., 2011). These modeling approaches lead to different results in terms of accuracy and computer time. For example, Monte Carlo based approaches tend to give very accurate results with very large computer times.

Atmosphere R.T. codes are usually divided into two families:

1) Line-by-line codes: they calculate the contribution of all atmosphere gasses, for each spectral line (Table 1).
2) Band transmission models: gas transmittance is defined as a mean value per spectral band (Table 2).

* Corresponding author. Tel.: +33 5 61 55 63 63.
E-mail addresses: eloi.grau@gmail.com (E. Grau), jean-philippe.gastellu-etchegorry@cesbio.cnes.fr (J.-P. Gastellu-Etchegorry).
[1] Tel.: +33 5 61 55 61 30.

0034-4257/$ – see front matter © 2013 Elsevier Inc. All rights reserved.
http://dx.doi.org/10.1016/j.rse.2013.07.019

Table 1
Examples of line-by-line atmospheric radiative transfer codes.

Model	Comment	Model reference
FASCODE	Voigt line shape decomposition and layering (Drayson, 1976)	Chetwynd, Wang, and Anderson (1994)
LBLRTM	Linear combination of fitting functions, derived from FASTCODE	Clough et al. (2005)
LinePak	No scattering	Gordley, Marshall, and Chu (1994)
GENLN2	No scattering	Edwards (1992)
4A	No scattering	Scott and Chedin (1981)

Most band transmission models treat landscapes as surfaces with a bidirectional reflectance, but neglect the spatial heterogeneity of these surfaces and the associated adjacency effects. Adjacency effects are due to radiation that is reflected or emitted by the target neighborhood and that reaches the sensor after one or several atmosphere scattering events, possibly after being backscattered by the atmosphere to the Earth surface. Models solve this problem with simplifying hypotheses. For example, they neglect the "Earth–Atmosphere radiative coupling" (i.e., radiation backscattered by the atmosphere to the Earth surfaces) or treat it as if the target neighborhood is a Lambertian surface (e.g., 6S and MODTRAN atmosphere models).

The usual way to retrieve Earth biophysical parameters (e.g. LAI: Leaf Area Index) from remote sensing (i.e., TOA: Top of the Atmosphere) images is to apply an atmosphere correction algorithm that transforms these images into Bottom of Atmosphere (BOA) images, and then to invert the BOA images with an Earth R.T. model. This approach can lead to large errors due to the difficulty to conduct accurate atmospheric corrections, especially if the land surface heterogeneity and the neighborhood effect are neglected or poorly taken into account. Terrestrial biophysical parameters can be also retrieved from the inversion of TOA images with a model that couples an Earth R.T. model and an atmosphere R.T. model (Laurent et al., 2011). In this case, the downward BOA fluxes generated by the atmospheric model must be an input of the Earth R.T. model, and the upward BOA fluxes generated by the Earth R.T. model must be an input of the atmosphere R.T. model. Due to the difficulty to implement this coupling, very simplifying hypotheses are usually assumed. Due to the difficulty to implement this coupling, some simplifying assumptions are usually made. For example, Verhoef and Bach (2003, 2007) apply a four-stream approximation of fluxes, which nevertheless turns out to be a powerful framework to describe the surface–atmosphere radiative interaction, allowing still to include the consideration of BRDF effects, surface heterogeneity and even adjacency effects.

Table 2
Examples of band transmission atmospheric radiative transfer codes.

Model	Principle of R.T. modeling	Reference
BandPak	Emissivity and transmittance pre-computed tables (no scattering)	Marshall and Gordley (1994)
SPCTRAL2	Analytic order 1	Bird and Riordan (1984)
MODTRAN	Correlated-k algorithm, includes DISORT	Berk & Bernstein (1999)
6S/6SV	Successive Order of Scattering (SOS) code	Vermote, Tanre, Deuze, Herman, and Morcrette (1997)
SBDART	Based on DISORT	Ricchiazzi, Yang, Gautier, and Sowle (1998)
Streamer	Based on DISORT	Key and Schweiger (1998)
Fluxnet	Neural network	Key and Schweiger (1998)
Fu Liou	2 and 4 streams	Fu and Liou (1993)
RRTM/RRTMG	Correlated-k algorithm	Mlawer, Taubman, Brown, Iacono, and Claugh (1997)
libRadtran	Based on SBDART	Mayer and Kylling (2005)
SCIATRAN	Correlated-k algorithm	Rozanov, Rozanov, Buchwitz, Kokhanovsky, and Burrows (2005)
KARINE	Monte Carlo	Eymet, Fournier, Blanco, and Dufresne (2004)
SHARM	Spherical harmonics	Lyapustin (2005)

The abovementioned works stress the complexity of the "Earth–Atmosphere" radiative coupling, especially if land surfaces are heterogeneous. It is very difficult to simulate accurately this coupling with the combined use of an Earth R.T. model and an atmosphere R.T. model if these models were not designed for such a coupling. In many cases, it can be simpler to design a fully integrated "Earth–Atmosphere" R.T. model. This is the option that we chose here: we included an atmosphere R.T. module within an existing land surface R.T. model, using compatible 2 R.T. modeling approaches. DART (Discrete Anisotropic Radiative Model) is the land surface R.T. model that is considered here (Gastellu-Etchegorry, 2008). The atmosphere R.T. module works on the same basis as DART. It is a band model that uses the discrete ordinate method with the flux tracking approach. It was first implemented by Gascon (2001) for simulating TOA reflectance and then by Martin (2006) for simulating TOA brightness temperature.

DART simulates remote sensing images and the spectral radiation budget of 1D/2D/3D natural and urban landscapes (e.g., trees, grass, and houses) from the visible to the thermal infrared domains. It was successfully tested with reflectance (Gastellu-Etchegorry & Zagolski, 1996) and temperature (Guillevic, Gastellu-Etchegorry, Demarty, & Prévot, 2003) measurements, and compared with other 3D models (Widlowski et al., 2008). It is developed since 1992 (Gastellu-Etchegorry & Zagolski, 1996) and is used in an increasing number of scientific works: 3D distribution of photosynthesis and primary production rates of vegetation canopies (Belot, 2007), forests (Barbier, Couteron, Proisy, Yadvinder, & Gastellu-Etchegorry, 2010; Couturier, Gastellu-Etchegorry, Patiño, & Martin, 2009; Malenovsky et al., 2008), urban areas (Gastellu-Etchegorry, 2008) and agriculture (Duthoit, Demarez, Gastellu-Etchegorry, Martin, & Roujean, 2008; Sepulcre-Cantó et al., 2009). It continues to be improved in terms of robustness, accuracy and functionality. Free licenses of present version 5.3.2 are available for scientists (http://www.cesbio.ups-tlse.fr/us/dart.html).

This paper presents recent improvements of the DART atmosphere R.T. modeling. Some of these improvements were requested by DART user scientists (Barbier et al., 2010; Sobrino, Mattar, Jiménez-Muñoza, Gastelllu-Etchegorry, & Grau, 2011; Timmermans, 2011) for obtaining in an easy way accurate simulations of TOA reflectance and brightness temperature of Earth surfaces. The first part of the paper summarizes basic points of DART model. The following section presents the new atmosphere R.T. module with its 4 modeling methods. (1) Use of transfer functions that "transmit" radiation from an atmosphere level (BOA, Sensor, TOA) to another one for decreasing computer times. (2) Automatic simulation of the atmosphere geometry for optimizing the "Computer time–Accuracy" trade-off of simulations. The last section presents the tests that were conducted for checking the robustness and accuracy of the DART atmosphere modeling. These tests were conducted with theoretical case studies and with comparisons with simulations of TOA radiance values by the MODTRAN4 model. The two appendices explain how the model (1) uses specific scattering points for an exact simulation of 1st order reflected and emitted radiation fluxes, (2) accounts of the Earth curvature on atmosphere radiation path lengths.

2. DART description

DART simulates radiative transfer in homogeneous and heterogeneous 1D, 2D and 3D scenes with the exact kernel and discrete ordinate methods. Any scene is simulated as a 3D array of rectangular cells (Δx, Δy, Δz). This array (Fig. 1) is a building block for simulating Earth scenes that are infinite and repetitive, possibly with atmosphere. DART is continuously improved in terms of accuracy, scene modeling (topography, foliar vertical and horizontal profiles within tree crowns,…), R.T. modeling (lidar, scene spectra, sensor broadbands,…) and functionality (SQL database,…). Some general principles of the first DART release

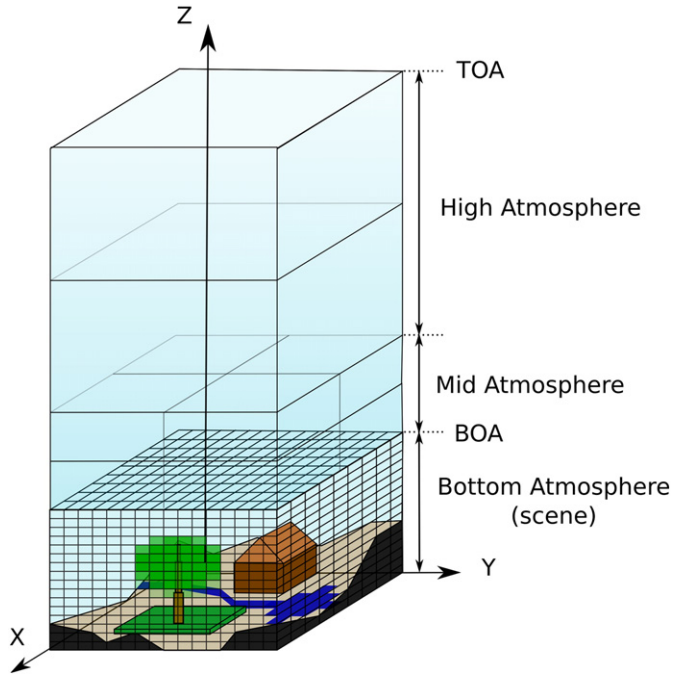

Fig. 1. Schematic representation of the geometry of the Earth–Atmosphere system. The atmosphere is made of 3 regions: Mid, High and bottom atmosphere. The atmosphere module that is presented here works with the mid and high atmospheres. The Earth landscape is within the bottom atmosphere.

(Gastellu-Etchegorry & Zagolski, 1996) are still used. The radiative transfer is solved using the discrete ordinate method, wherein radiation is restricted to propagate in a finite number of directions (Ω_i) with an angular sector width ($\Delta\Omega_i$) (sr). Any set of N discrete directions can be used (solid angles are not necessarily equal, but $\sum_{n=1}^{N}\Delta\Omega_n = 4\pi$). DART precomputes the discretization of directions in order to have homogeneous directions (Yin et al., 2012), and the landscape geometrical representation.

DART works with spectral intervals (so called "spectral bands"), with mean optical properties. Several spectral bands can be computed in one simulation. Any radiation that propagates along direction (Ω_i) at a position r is called a source vector $W(r,\Omega_i)$ [W/m]. Radiative transfer equation in the Cartesian coordinate system can be written as:

$$\left[\xi\frac{d}{dx}+\eta\frac{d}{dy}+\mu\frac{d}{dz}\right].L(r,\Omega_n) = -\alpha_e(r,\Omega_n).L(r,\Omega_n)+\alpha_a(r,\Omega_n).L_B(r,\Omega_n)+\sum_{m=1}^{N}\alpha_d(r,\Omega_n).\frac{P(r,\Omega_m\rightarrow\Omega_n)}{4\pi}.L(r,\Omega_n).\Delta\Omega_n$$

where ξ, η and μ are the cosine of the direction Ω_n according to x, y and z, α_e, α_a and α_d are respectively the extinction, absorption and scattering coefficients of the medium, $L(r,\Omega_n)$ is the radiance at point r along direction Ω_n [W/m^2/sr/m], and $\frac{P(r,\Omega_m\rightarrow\Omega_n)}{4\pi}$ the phase function of the medium.

Earth scene BOA irradiance has 2 components: the direct sun $W(\Omega_s)$ and atmosphere $W_a(\Omega_n)$ source vectors. They are assumed to originate from a fictitious level at the top of the scene (BOA). Direct sun source vectors propagate along the direction (Ω_s), with θ_s and ϕ_s the sun zenith and azimuth angles. At the top of the scene:

$$W(\Omega_s) = E_s(\Omega_s).|\mu_s|.\Delta x.\Delta y \quad W_a(\Omega_n) = L_a(\Omega_n).|\mu_n|.\Delta x.\Delta y.\Delta\Omega_n \quad [W/m]$$

where $\mu_s = \cos\theta_s$, $\mu_n = \cos\theta_n$, $\Delta x.\Delta y$ is the cell face area. $E_s(\Omega_s)$ [W/m^2/m] is the direct solar irradiance at the top of the scene. $L_a(\Omega_n)$ is the atmospheric radiance [W/m^2/sr/m] along direction (Ω_n), with $n \in [1\ N']$, with N' the number of downward discrete directions. It is due to atmosphere scattering and/or thermal emission.

DART cells can contain turbid material and triangles. Turbid material is used for simulating volumic (3D) interactions (vegetation and air), with propagation of radiation obeying to Beer's law. For example, a tree crown is the juxtaposition of a set of "turbid" cells. On the other hand, triangles are used for simulating surface (2D) interactions (trunks, branches, walls, topography,…). The schematic way a vegetation cell interacts with an incident ray is presented here because it will ease the understanding of the interaction of air cells with radiation, in the following section. Similarly to air cells, a vegetation cell is treated as a turbid medium where radiation attenuation follows the Beer law (Ross, 1981). Let $C(l,\Omega_s)$ be a source vector that propagates through a vegetation cell i along a direction Ω_s, where $l \in [0\ \Delta l_i]$ is the path length from the entrance point (A) of cell i, and Δl_i the within cell path length. Propagation of $W(l,\Omega_s)$ gives rise to within cell scattered source vectors $W_1(\Delta l_i,\Omega_s \rightarrow \Omega_v)$ along the N discrete directions (Ω_v, $\Delta\Omega_v$), $v \in [1\ N]$. Cell scattering along (Ω_v) is computed with the assumption that source vectors $W_1(\Delta l_i,\Omega_s \rightarrow \Omega_v)$ originate from a finite number of points (x, y, z), called middle point (M_s(x, y, z)), within the cell i. Simulation of scattering mechanisms from adequately located (M_s) points, instead of a single point such as the cell center, improves the accuracy of results, especially for cells with large foliar volume densities and for oblique propagation directions. For example, a vector source that exits a cell with a very large density value after being scattered is nearly zero if it is simulated from the cell center, which is usually wrong. In order to take into account the fact that several source vectors propagate through each cell, one uses points, also called M_s, that are the center of gravity of individual points M_s.

The single-scattering radiation $W_{1,out}(\Delta l_i,\Omega_s \rightarrow \Omega_v)$ that exits the cell along (Ω_v) corresponds to the attenuation of within cell single scattered energy W_1 $(\Delta l_i,\Omega_s \rightarrow \Omega_v)$ after a propagation length $\Delta s(\Omega_v)$ from point M_s.

$$W_{1,out}(\Delta l,\Omega_s\rightarrow\Omega_v) = W_1(\Delta l,\Omega_s\rightarrow\Omega_v).\exp[-G(j,\Omega_v).u_f(i).\Delta s(\Omega_v)]$$

with $G(j,\Omega_v)$ the effective foliar cross section per leaf area and u_f the cell foliar volume density.

Within cell multiple scattering $W_M(\Delta l_i,\Omega_s \rightarrow \Omega_v)$ is due to the energy $W_{1,int}(\Delta l_i,\Omega_s \rightarrow \Omega_v)$ that is intercepted along the path $\Delta s_i(\Omega_v)$ from M_s to the external boundary of cell i. Because it cannot be modeled exactly, two approximations are used: (1) total outgoing radiation that has undergone more than one scattering within a cell is modelized with a geometrical series (as it is proportional to the albedo of the vegetation, the total intercepted energy during first order scattering and mean transmittance of the cell Gastellu-Etchegorry & Zagolski, 1996), and (2) $W_M(\Delta l_i,\Omega_s \rightarrow \Omega_v)$ is proportional to $W_1(\Delta l_i,\Omega_s \rightarrow \Omega_v)$. Finally, the total scattered source vector, i.e. single and within cell multiple scattering radiation, along direction (Ω_v) is:

$$W_1(\Delta l_i,\Omega_s\rightarrow\Omega_v) + W_M(\Delta l_i,\Omega_s\rightarrow\Omega_v).$$

DART's potential for simulating images is illustrated here with simulated color composites (Fig. 2) of a schematic hilly countryside landscape and a schematic peri-urban landscape. They were simulated with the atmosphere R.T. modeling presented in this paper, in the blue, green and red spectral domains, at the bottom (BOA) and top (TOA) of the atmosphere. All elements (trees, house,…) of the countryside scene are directly simulated by DART, whereas some elements of the urban scene are imported. For example, the tree of the urban scene comes from the 4th phase of the RAMI experiment (Widlowski et al., 2008).

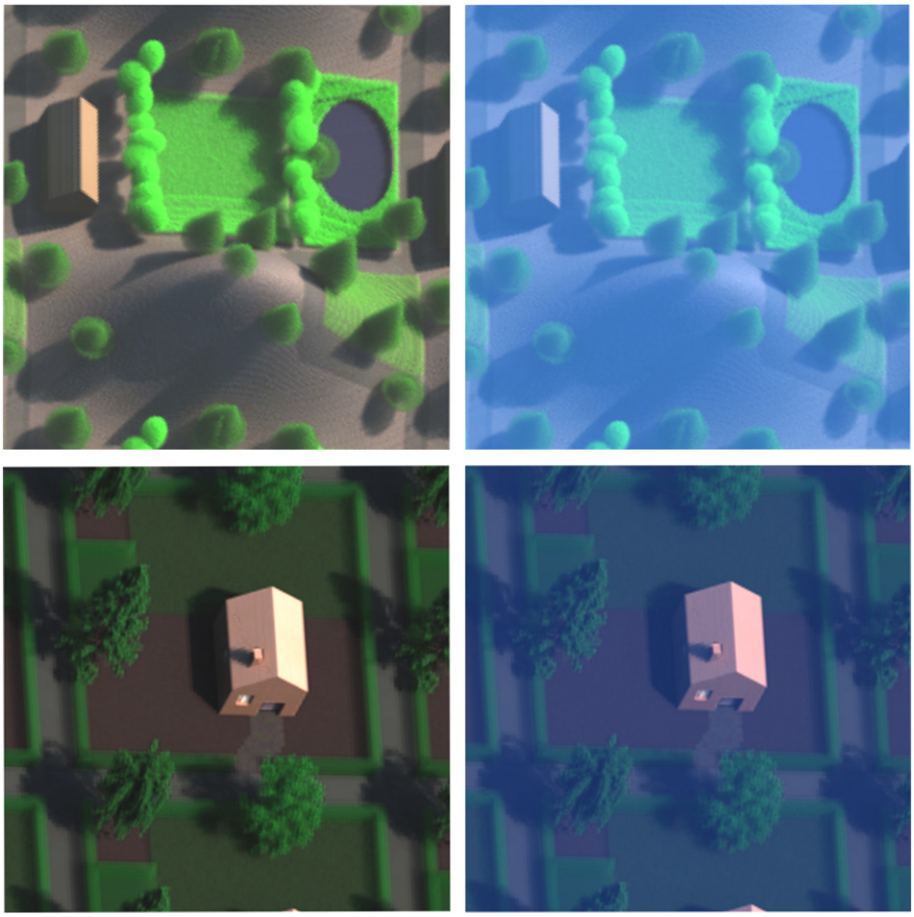

Fig. 2. DART color composite images of schematic landscapes, for an oblique view direction. BOA (left) and TOA (right) levels. Top: Schematic hilly countryside landscape with elements (trees, road, lake, agriculture plots,…) generated by DART. Bottom: Schematic urban landscape with elements (houses, trees) imported by DART, and generated by DART (grass, hedges, roads).

3. Atmosphere radiative transfer modeling

3.1. Simulation of the atmosphere

Similarly to its Earth scene R.T. modeling, DART models the atmosphere R.T., with "ray tracing" and "discrete ordinates" approaches. The atmosphere is considered as the vertical and horizontal juxtaposition of air cells. It contains gasses and aerosols, only. There are no clouds. Each air cell has specific optical properties. At the exception of the bottom atmosphere (BA), optical properties are horizontally homogeneous. Gasses and aerosols are accounted separately with specific phase functions (i.e., $P_{gas}(\Psi)$, $P_{aerosol}(\Psi)$) and extinction coefficients for scattering and absorption (i.e., $\alpha^{abs}_{aerosol}(\lambda)$, $\alpha^{scat}_{aerosol}(\lambda)$, $\alpha^{abs}_{gas}(\lambda)$, $\alpha^{abs}_{gas}(\lambda)$), where Ψ is the phase angle between the incident and the scattered directions, and λ is the wavelength.

The atmosphere is divided into 3 superimposed zones that are simulated as matrices of air cells. As already mentioned, each air cell is characterized by 2 extinction coefficients (α) and 2 single scattering albedos (ω): 2 for gasses (α_{gas}, ω_{gas}) and 2 for aerosols ($\alpha_{aerosol}$, $\omega_{aerosol}$). Each atmosphere zone (BA, MA, HA) has a specific sampling grid ($\Delta x = \Delta y$, Δz), which allows one to use a coarser sampling grid for MA, than for BA, where atmosphere density is larger:

- Bottom Atmosphere (BA). Air cell sizes are equal to those of the cells that are used for simulating the Earth landscape. Usually, they are defined in relation with the dimensions of the objects that make up the Earth landscape and the spatial resolution of simulated images. Their optical properties can show a 3D variability. Simulation of BA air cells is useful with very large landscapes (e.g., entire valley) and in the presence of pollution.
- Mid Atmosphere (MA). Air cells can have any horizontal sizes, smaller than the landscape cell sizes. Their vertical number and dimension can be specified by the user or can be computed automatically with an approach described later. The distribution of optical properties is horizontally homogeneous. MA is the atmosphere zone that contributes to the heterogeneous "Earth–Atmosphere" coupling. Its optical depth is noted τ_{MA}.
- High Atmosphere (HA). It is a superimposition of layers (i.e., cells with a horizontal size equal to the dimension of the scene). The vertical size and number of layers are specified by the user or computed automatically. The optical depth of HA is noted τ_{HA}.

DART store radiance at 4 levels: (1) "level TOA" at the top boundary of HA. Its top default altitude is $h_{TOA} = 100$ km. (2) "Level MA–HA" and (3) "Level BOA" at the top and bottom boundaries of MA, respectively. The altitude of level MA–HA is noted h_{MA-HA}. (4) "Level Sensor" at the sensor level (i.e., any altitude between the BOA and TOA levels). In these levels, energy is stored per direction and per pixel. The pre-computation of transfer functions is used to propagate energy from a level to another, in order to accelerate computation time.

One can input manually the atmosphere characteristics, or DART can compute them with 2 spectral and geometric atmosphere databases that were built up with the MODTRAN atmosphere model (Berk & Bernstein, 1989) for a number of classical gas and aerosol models. The first database stores the TOA extraterrestrial solar spectral irradiance

(Kurucz solar source function, in W/m^2/m), with 1 cm^{-1} resolution, from 0.25 μm up to 1000 μm.

The second database stores:

* 7 gas models: 6 classical gas models (i.e., US Standard 1976, Tropical, Mid-Latitude Summer, Mid-Latitude Winter, Sub-Arctic Summer, Sub-Arctic Winter) and a user defined model which allows the user to input his own data. For each gas model, the database stores:
  - Total gas spectral transmittance $T^{\uparrow}_{gas,abs}(\lambda)$ due to absorption in an up and down atmosphere vertical path,
  - Total single scattering albedo $\omega_{gas}(\lambda)$, direct transmittance $T^{\downarrow}_{gas,scat}(\lambda)$ and scale height H_{gas} of all scattering gasses.
  - Vertical transmittance $T^{\downarrow}_{gas,x,abs}(\lambda)$ and height factor H_x of each gas x among the 7 major absorbing gasses (i.e., N_2, O_2, CO_2, H_2O, CO, CH_4),
  - Vertical transmittance $T^{\downarrow}_{O_3}(\lambda)$ and density distribution $d_{O_3}(z)$ of ozone.
  - Total vertical transmittance $T^{\downarrow}_{17,abs}(\lambda)$ and density distribution $d_{17}(z)$ of the 17 minor absorbing gasses: NH_3, NO, NO_2, SO_2, CFC11, CFC_{12}, CFC_{13}, CFC_{14}, CFC_{22}, CFC_{113}, CFC_{114}, CFC_{115}, $CLONO_2$, HNO_4, $CHCL_2F$, CCL_4, N_2O_5.
  - Vertical transmittance $T^{\downarrow}_{H_2O,abs}(\lambda)$ of water vapor for water thicknesses from 0 cm up to 5 cm. In the database that is provided with DART model, it corresponds to a US Standard gas model.
  - 1D temperature vertical profile $T_{atm}(z)$, for each of the 7 gas models. Scale height H_{gas} is used to distribute gasses, other than ozone and the set of 17 absorbing gasses, with an exponential vertical profile. For example, at the altitude z, a gas with a spectral transmittance $T_{gas}(\lambda)$ and a scale height H_{gas} has an extinction coefficient equal to:

$$\alpha_{gas}(\lambda, z) = \frac{-\ln\left[T_{gas}(\lambda)\right]}{H_{gas}} \cdot \exp\left(-\frac{z}{H_{gas}}\right).$$

The spectrally integrated coupled path transmittance $T^{\uparrow}_{gas,abs}(\lambda)$ is stored because in finite spectral bands that contain strong absorption lines it is not equal to the product $T^{\downarrow}_{gas,abs}(\lambda)$. $T^{\uparrow}_{gas,abs}(\lambda)$ of spectrally integrated path transmittances (Berk & Bernstein, 1999). Indeed, in these spectral bands, radiation propagation does not follow the Beer law (cf Section 4.1). Use of $T^{\uparrow}_{gas,abs}(\lambda)$ allows one to use the Beer law for simulating TOA signals, whereas $T^{\downarrow}_{gas,abs}(\lambda)$ is used for computing BOA radiative products in the sun radiation domain. The approach relies on extinction coefficients that take into account the values of $T^{\uparrow}_{gas,abs}(\lambda)$ and $T^{\downarrow}_{gas,abs}(\lambda)$ values. The latter ones are derived from MODTRAN simulations with a 1 cm^{-1} spectral resolution and a vertical sun direction. For downward radiation, gas extinction coefficients are derived from $T^{\downarrow}_{gas,abs}(\lambda)$ values, which ensure that DART and MODTRAN give the same direct downward vertical radiance, at BOA level. For upward radiation, gas extinction coefficients are derived from $T^{\uparrow}_{gas,abs}(\lambda)$ values, which ensure that DART and MODTRAN give the same direct upward vertical radiance, at TOA level. For oblique sun and view directions, this approach tends to be less accurate in spectral domains with strongly varying spectral properties. Indeed, in these domains, the atmosphere direct transmittance along an oblique view direction with a zenith angle θ is not exactly equal to the atmosphere direct vertical transmittance power 1/cosθ. A possible solution could be to compute $T^{\uparrow}_{gas,abs}(\lambda)$ and $T^{\downarrow}_{gas,abs}(\lambda)$ for a set of oblique directions. It is not used in DART because most remote sensing measurements are performed for not too oblique view directions and for spectral bands with as few strong absorption lines as possible.

The angular distribution of gas scattering is simulated with the Rayleigh phase function formula given by Chandrasekhar (1960):

$$\frac{P_R(\Psi_{sv})}{4\pi} \simeq \frac{3(1-\delta)}{2(2+\delta)} \cdot \left(\frac{1+\delta}{1-\delta} + \cos^2\Psi_{sv}\right)$$

where Ψ_{sv} is the phase angle between the incident direction Ω_s and the scattering direction Ω_v. δ is the depolarization factor. A constant value (i.e., δ = 0.0279) is used for the optical domain (Bulcholtz, 1995; Young, 1980).

* 7 aerosol models: 6 classical aerosol models (i.e., Rural with a visibility V = 23 km and V = 5 km, Maritime with V = 23 km, Urban with V = 5 km, Troposphere with V = 50 km, Fog with V = 0.5 km) and a user defined aerosol model. For each aerosol model, the database stores:
  - Aerosol direct vertical transmittance $T_{aerosol}(\lambda)$,
  - Mean single scattering albedo $\omega_{aerosol}(\lambda)$,
  - Density scale height $H_{aerosol}$, for simulating an exponential vertical distribution, and vertical density distribution $d_{aerosol}(z)$, for simulating a vertical distribution that is not necessarily exponential.
  - 3 parameters (a, g_1, g_2) that characterize the double Henyey–Greenstein functions that define the aerosol phase function $P_{aerosol}(\Psi)$:

$$P_{aerosol}(\Psi) = \frac{a.\left(1-g_1^2\right)}{\left[1+g_1^2-2.g_1\cos(\Psi)\right]^{1.5}} + \frac{(1-a).\left(1-g_2^2\right)}{\left[1+g_2^2-2.g_2\cos(\pi-\Psi)\right]^{1.5}}.$$

3.2. Pre computation

Before simulating the R.T. in the "Earth–Atmosphere" system, three types of geometric and spectral quantities of the atmosphere are pre-computed:

- *Atmosphere geometry*: altitude of level "MA–HA", MA cell dimensions and HA cell vertical dimension. These quantities are computed in order to meet the best "Computer time–Pre-defined accuracy value on atmosphere reflectance or brightness temperature" trade-off, as explained later.
- *TOA sun irradiance*: it is computed with the DART atmosphere database, the date (Julian day and time) and the sensor and Earth surface locations (latitude, longitude).
- *Atmosphere optical properties*: gas and aerosol extinction coefficients at any altitude of each atmosphere layer.

In addition, DART pre-computes 8 atmosphere transfer functions (TF). These TFs are designed in order to decrease a lot computer time. Indeed, they avoid to simulate the atmosphere R.T. with repetitive computations that are necessarily identical because the MA and HA zones are horizontally homogeneous. They are defined per spectral band and per upward direction. There are four types of TFs:

- TF from level MA–HA to any level. It is used to simulate direct propagation of radiation through HA (upward directions) and MA (downward direction) from the level MA–HA. It stores intercepted energy per layer and direct transmitted energy. It is used for computing the other atmosphere radiative transfer functions.
- $TF^{dir}_{BOA,layer}$: 2 "direct" TFs store direct transmittance values. Each TF gives the energy and position of a ray from BOA level that reaches "Sensor" or "TOA" level along direction $(\Omega^{\uparrow}_s)$.
- $TF^{scat}_{BOA,layer}$: 4 "diffuse" TFs store scattering transmittance from BOA level (i.e., upward radiation) to BOA and Sensor levels (i.e., downward radiation) and to TOA and Sensor levels (i.e., upward radiation).
- TF^{abs}: 1 "absorption" TF stores the energy that is absorbed in the MA and HA layers when a unit ray $W_{BOA}(\Omega^{\uparrow}_s)$ directly crosses the atmosphere, starting from the BOA level.

Transfer functions TF^{dir}, TF^{scat} and TF^{abs} are convolved with BOA upward radiation $W_{BOA}(\Omega_s^{\uparrow})$ for simulating remote sensing images. It must be noted that this approach takes into account the fact that radiance from Earth surfaces is not spatially homogeneous and not isotropic. Once computed, these TFs can be applied to any DART simulation where the atmosphere has the same properties. This avoids one to compute again optical properties, which reduces computer times.

Direct and diffuse TF are defined for a flux $W_{BOA}(\Omega_s^{\uparrow})$ that leaves the level BOA along direction $(\Omega_s^{\uparrow})$ at the pixel (i,j). $TF^{scat}_{BOA,layer}$ are sampled at the MA horizontal resolution because MA scattering is driven by the digitizing grid of MA. More specifically, $TF^{scat}_{BOA,layer}$ functions give the ray that reaches a level at pixel (i′,j′) in any direction ($\Omega_v^{\downarrow}$ or $\Omega_v^{\uparrow}$), due to an upward ray $W_{BOA}(\Omega_s^{\uparrow})$ that leaves the BOA level at point (i,j) along any upward direction $(\Omega_s^{\uparrow})$.

Direct, diffuse and absorption transfer functions are listed below, with the notation $\Delta i = i' - i$ and $\Delta j = j - j'$:

$TF^{dir}_{BOA,TOA}(\Delta i,\Delta j,\Omega_s^{\uparrow},\Omega_s^{\uparrow})$: direct (no scattering) flux up to each cell (i′,j′) of TOA level, along each direct direction $\Omega_s^{\uparrow}$.
$TF^{dir}_{BOA,Sensor}(\Delta i,\Delta j,\Omega_s^{\uparrow},\Omega_s^{\uparrow})$: direct (no scattering) flux up to each cell (i′,j′) of Sensor level, along each upward direction $\Omega_s^{\uparrow}$.
$TF^{scat}_{BOA,BOA}(\Delta i,\Delta j,\Omega_s^{\uparrow},\Omega_v^{\downarrow})$: backscattered flux from BOA down to any cell (i′,j′) of BOA level, for each downward direction $\Omega_v^{\downarrow}$, for each initial direction $(\Omega_s^{\uparrow})$.
$TF^{dir}_{BOA,TOA}(\Delta i,\Delta j,\Omega_s^{\uparrow},\Omega_v^{\uparrow})$: energy scattered from BOA up to each cell (i′,j′) of TOA level, along each upward direction $\Omega_v^{\uparrow}$, for each initial direction $(\Omega_s^{\uparrow})$.
$TF^{scat}_{BOA,Sensor}(\Delta i,\Delta j,\Omega_s^{\uparrow},\Omega_v^{\downarrow})$: energy backscattered from BOA down to each cell (i′,j′) of Sensor level, along each downward direction $\Omega_v^{\downarrow}$, for each initial direction $(\Omega_s^{\uparrow})$.
$TF^{scat}_{BOA,Sensor}(\Delta i,\Delta j,\Omega_s^{\uparrow},\Omega_v^{\uparrow})$: energy scattered from BOA up to each cell (i′,j′) of "Sensor" level, along each upward direction $\Omega_v^{\uparrow}$, for each initial direction $(\Omega_s^{\uparrow})$.
$TF^{abs}_{MA}(n,\Omega_s^{\uparrow})$: absorbed energy per layer n of the MA atmosphere.
$TF^{abs}_{HA}(n,\Omega_s^{\uparrow})$: absorbed energy per layer n of the HA atmosphere.

The computation of these TFs (Fig. 3) relies on atmosphere R.T. modeling. It starts with an upward ray W $(\Omega_s^{\uparrow})$ that exits the level BOA. Its direct transmission gives rise to radiation interception in MA and HA zones. Scattering of this radiation is simulated with an iterative procedure: radiation that is intercepted at iteration (i) is scattered at iteration (i + 1). The number of iterations can be modified in order to manage the accuracy of TFs. At every iteration, scattering is simulated in 4 steps. These 4 steps are repeated until total energy to scatter in the atmosphere is less than a threshold value or if a maximum number of iterations is reached. For example, atmosphere scattering during the so-called "Sun illumination stage", in the absence of Earth surfaces, is simulated with an iterative procedure where each iteration is made of the 4 steps:

1) Scattering of radiation that was intercepted in HA during direct illumination. It gives rise to intercepted radiation in HA and radiation that is incident on levels TOA and MA-HA.
2) Downward illumination of MA (with HA–MA to BA transfer function) due to the downward radiation that was stored on level MA–HA at step 1. It gives rise to intercepted radiation in MA and downward radiation that is incident on BOA level.
3) Scattering of radiation that was intercepted in MA. This gives rise to intercepted radiation in MA and radiation that is incident on BOA and MA–HA levels.
4) Upward illumination of HA (with HA–MA to TOA transfer function) by the upward radiation that is stored in the MA–HA level during step 3 of the present iteration.

3.3. Radiative transfer in the Earth–Atmosphere system

DART simulates the radiative transfer in the "Earth–Atmosphere" system in 5 stages (Fig. 4):

- Stage 1: Illumination stage: computation of TOA and BOA atmospheric irradiance (sun irradiance and/or atmosphere thermal emission and scattering).
- Stage 2: Landscape R.T. with/without landscape thermal emission.
- Stage 3: Atmosphere backscattering down to the landscape of the upward radiation calculated at stage 2.
- Stage 4: Landscape R.T. of the radiation that the atmosphere backscatters by at stage 3.
- Stage 5: Transfer of upward fluxes (stages 2 and 4) from the BOA level to the TOA and Sensor levels.

These 5 stages are presented below.

•*Stage 1: Earth illumination*. Stage 1 computes the Earth radiation regime for the selected DART mode. For the reflectance mode "R", the

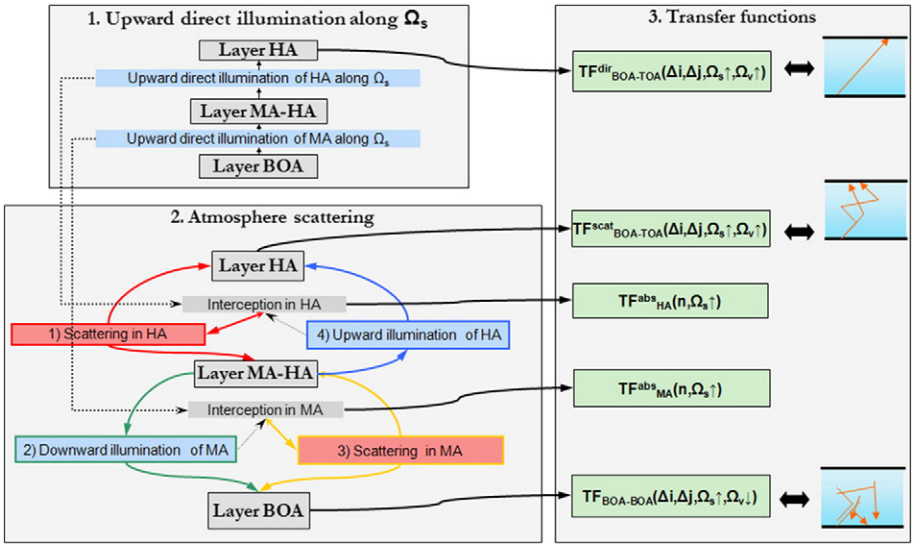

Fig. 3. Algorithm for computing atmosphere transfer functions for each upward direction $\Omega_s^{\uparrow}$. Transfer functions associated to the "Sensor" layer are not shown.

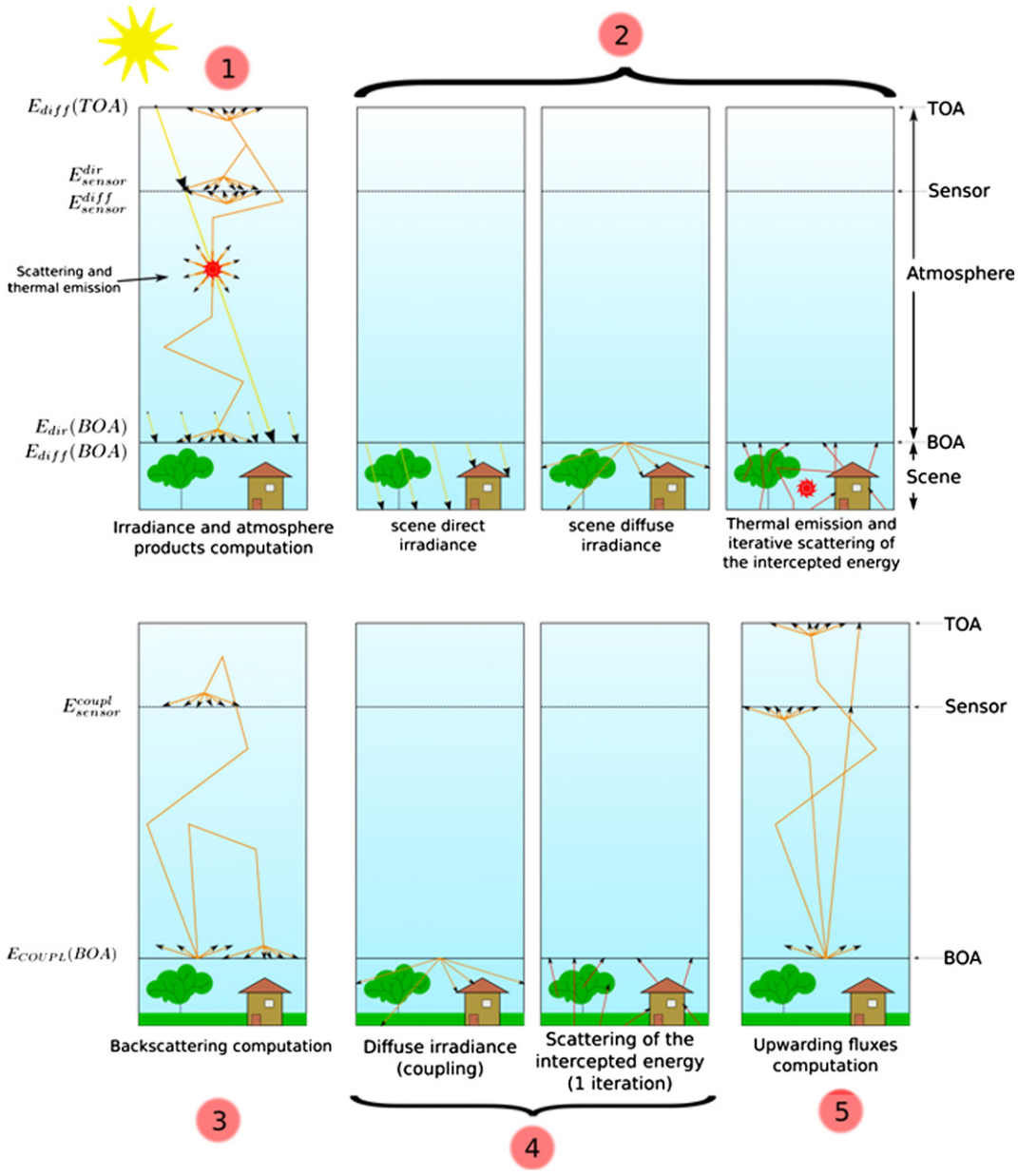

Fig. 4. Schematic view of the 5 stages of the algorithm that models the R.T. in the "Atmosphere–Earth" system.

Earth is illuminated by the sun radiation that crosses the atmosphere without interaction and by sun radiation that is scattered by the atmosphere. In the thermal emission mode "T", the atmosphere emits and illuminates the Earth. Moreover, the Earth emits also. The third DART mode (i.e., mode "R + T") combines methods of DART modes "R" and "T": the Earth is illuminated by the sun, by downward atmosphere scattering and by downward atmosphere emission. During this stage, the atmosphere is simply simulated as the superimposition of layers, because it is assumed to be horizontally homogeneous and because the Earth surface heterogeneity has no influence at this stage.

Only, the 1st phase of stage 1 (thermal emission and/or direct sun illumination) depends on DART mode. Phase 2 (atmosphere scattering) of stage 1 computes HA and MA scattering with a 4 step algorithm (Fig. 5) that is similar to the algorithm used for computing the TFs (Fig. 3).

Phase 1:

- Modes "R" and "R + T": Downward direct sun flux first crosses HA, and then MA. The energy intercepted in HA and MA is stored for further scattering in Phase 2.
- Modes "T" and "R + T":

a) Emission of HA: it gives rise to radiation interception in HA and radiation incident on TOA and HA–MA levels.

b) Emission of MA: it gives rise to radiation interception in MA and radiation incident on BOA and HA–MA levels.

Phase 2: Iterative HA and MA scattering of radiation already intercepted and not yet scattered. In the thermal domain, a quasi-convergence is reached with a single iteration. Finally, one gets the downward radiance $L_{BOA}(\Omega)$ at BOA level, the upward $L_{sensor}(\Omega^{\uparrow})$ and downward $L_{sensor}(\Omega^{\downarrow})$ radiance at sensor level, and the upward radiance $L_{TOA}(\Omega^{\uparrow})$ at TOA level. These

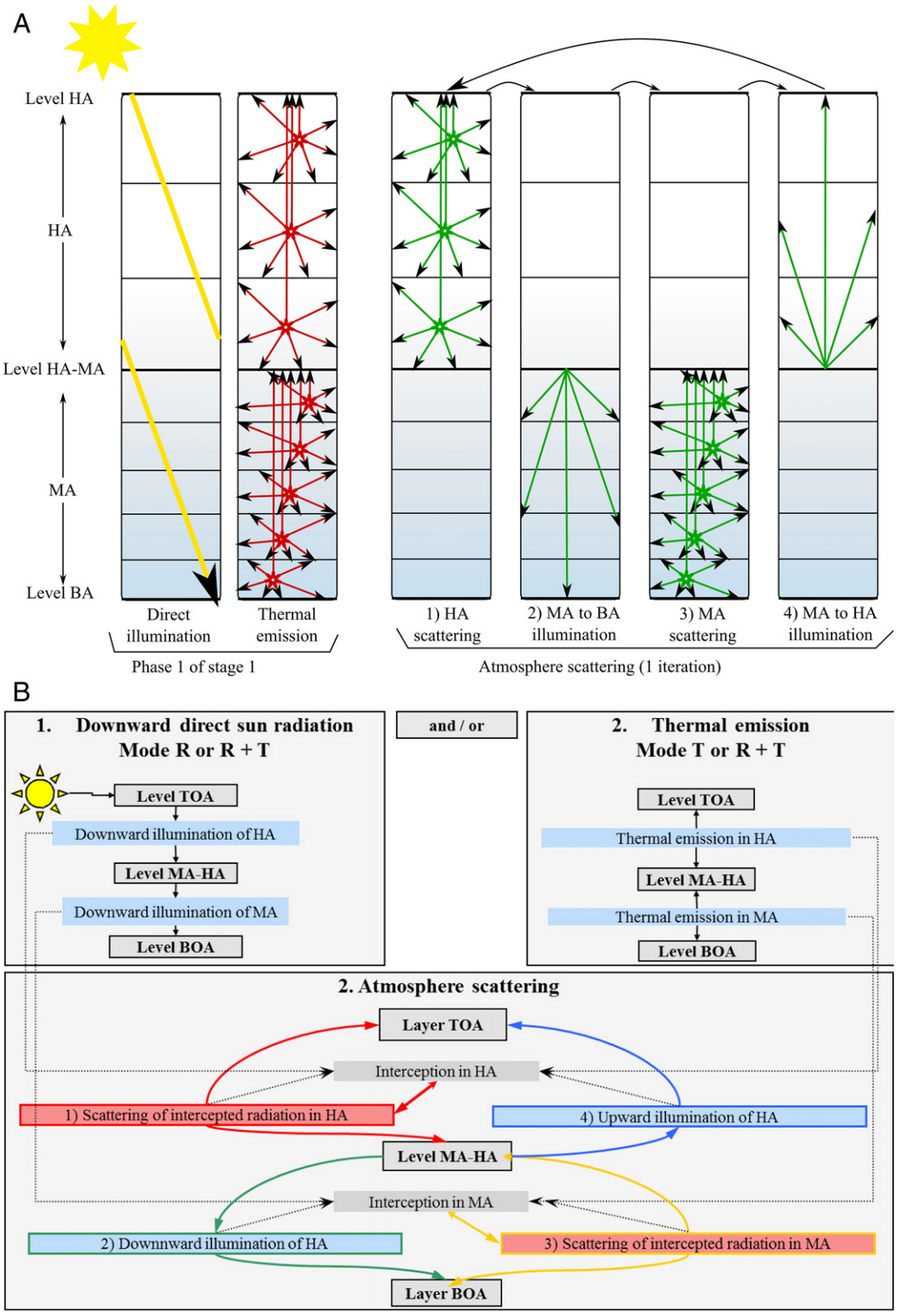

Fig. 5. DART "Sun illumination" stage. A) Schematic atmosphere: 3 layers for HA and 5 layers for MA. First, direct sun illumination (phase 1 of stage 1 in DART modes "R" and "R + T") gives rise to radiation intercepted (red stars) in HA and MA. This gives scattering, possibly combined with thermal emission, which leads to interception and scattering, and so on. After a few iterations, one gets the upward radiance at TOA level and the downward radiance at BOA level. Radiation incident on layers "BOA" and TOA is homogeneously (spatially) distributed on these horizontal layers. B) Algorithm.

quantities are used to compute the atmosphere reflectance (or brightness temperature) at sensor level $\rho_{atm,sensor}(\Omega_s,\Omega_v)$ and TOA level $\rho_{atm}(\Omega_s,\Omega_v)$.

•Stage 2: *Radiative transfer in the Earth landscape and possibly in the air (layer BOA)*. R.T. in the Earth scene, possibly with BA air cells, gives the scene upward radiance $L_{BOA}(i,j,\Omega^{\uparrow})$ for any pixel (i,j)

of BOA level. The associated spectral Earth hemispheric albedo q (i.e. the total upwarding energy divided by the total downwarding energy at BOA level) stored is used in stage 3:

$$q = \frac{\Sigma_i \Sigma_j \Sigma_{2\pi} + L_{BOA}\left(i, j, \Omega^{\uparrow}\right).\cos(\theta).\Delta x.\Delta y}{\Sigma_i \Sigma_j \Sigma_{2\pi} - L_{BOA}\left(i, j, \Omega'^{\downarrow}\right).\cos(\theta').\Delta x.\Delta y}$$

•Stage 3: *Atmosphere backscattering of the upward radiation scattered in stage 2*. The atmosphere backscatters radiation down to the BOA and sensor levels. In order to decrease computer time, this atmosphere backscattering is calculated by convolving the upward radiation $W_{BOA}(i,j,\Omega^{\uparrow})$ that exits a pixel (i,j) of BOA level along an upward direction $\Omega^{\uparrow}$, with the 2 pre-computed transfer functions: $TF_{BOA,BOA}^{scat}(\Delta i,\Delta j,\Omega^{\uparrow},\Omega'^{\downarrow})$ and $TF_{BOA,Sensor}^{scat}(\Delta i,\Delta j,\Omega^{\uparrow},\Omega'^{\downarrow})$. As these TFs are sampled at MA cell size, the fluxes $W_{BOA}(i,j,\Omega^{\uparrow})$ are sub-sampled at MA cell size, then convolved, and finally oversampled at BA grid with a classical bilinear method.

Each pixel (i′,j′) at BOA or Sensor level in the downward direction $\Omega'^{\downarrow}$ is affected by each upwarding flux from any pixel (i,j) at BOA level in any upwarding direction $\Omega^{\uparrow}$ scattered by the atmosphere, so:

Downward flux at Sensor level:

$$W_{Sensor}\left(i', j', \Omega'^{\downarrow}\right) = \sum_i \sum_j \sum_{\Omega^{\uparrow}} W_{BOA}\left(i, j, \Omega^{\uparrow}\right).TF_{BOA,Sensor}^{scat}\left(\Delta i, \Delta j, \Omega^{\uparrow}, \Omega'^{\downarrow}\right)$$

Downward flux at BOA level:

$$W_{BOA}\left(i', j', \Omega'^{\downarrow}\right) = \sum_i \sum_j \sum_{\Omega^{\uparrow}} W_{BOA}\left(i, j, \Omega^{\uparrow}\right).TF_{BOA,BOA}^{scat}\left(\Delta i, \Delta j, \Omega^{\uparrow}, \Omega'^{\downarrow}\right).$$

The associated spectral atmosphere backscattering (i.e. the total downwarding energy divided by the total upwarding energy at BOA level) albedo is:

$$s = \frac{\sum_i \sum_j \sum_{2\pi^-} L_{BOA}\left(i, j, \Omega'^{\downarrow}\right).\cos\left(\theta'\right).\Delta x.\Delta y}{\sum_i \sum_j \sum_{2\pi^+} L_{BOA}(i, j, \Omega^{\uparrow}).\cos(\theta).\Delta x.\Delta y}.$$

Actually, there is an endless succession of "Atmosphere backscattering–Earth upward scattering" events, with a decreasing importance. Here, the successive irradiance values are assumed to form a geometric series. Thus, we have:

$$W_{BOA}\left(i', j', \Omega'^{\downarrow}\right) = \frac{1}{1-q.s}.\sum_i \sum_j \sum_{\Omega^{\uparrow}} W_{BOA}\left(i, j, \Omega^{\uparrow}\right).TF_{BOA,BOA}^{scat}\left(\Delta i, \Delta j, \Omega^{\uparrow}, \Omega'^{\downarrow}\right).$$

•Stage 4: *Radiative transfer of the backscattered radiation within the Earth landscape*. Similarly to stage 2, the Earth landscape scatters the downward radiation $W_{BOA}(i,j,\Omega^{\downarrow})$ that is computed at stage 3 for each pixel (i,j) of BOA level. Stage 4 is conducted with a single iteration that is extrapolated using a multiplicative factor that is computed at stage 2:

$$\frac{\text{Extrapolated scene excitance, at stage 2}}{\text{Scene excitance after 1 iteration, at stage 2}}.$$

The use of this extrapolation instead of computing exactly the extrapolation is justified by the fact that radiation is much smaller in stage 4 than in stage 2.

•Stage 5: *Radiation at sensor and TOA levels*. The transfer functions $TF_{BOA-TOA}$ and $TF_{BOA-Sensor}$ used for computing TOA and sensor images are derived from $\{TF_{BOA,TOA}^{dir}, TF_{BOA,TOA}^{scat}\}$, and $\{TF_{BOA,Sensor}^{dir}, TF_{BOA,Sensor}^{scat}\}$, respectively.

Upward flux at TOA level: "Upward Flux from BOA" × "Transfer Functions $TF_{BOA-TOA}(\Delta i,\Delta j,\Omega^{\uparrow},\Omega'^{\uparrow})$"

$$W_{TOA}\left(i', j', \Omega'^{\uparrow}\right) = \sum_i \sum_j \sum_{\Omega^{\uparrow}} W_{BOA}\left(i, j, \Omega^{\uparrow}\right).TF_{BOA,TOA}\left(\Delta i, \Delta j, \Omega^{\uparrow}, \Omega'^{\uparrow}\right)$$

Function $TF_{BOA-TOA}(\Delta i,\Delta j,\Omega^{\uparrow},\Omega'^{\uparrow})$ gives the upward flux $W_{TOA}(i',j',\Omega^{\uparrow})$ for any upward direction $\Omega'^{\uparrow}$ for any pixel (i′,j′) at sensor level, due to a unit flux $W_{BOA}(i,j,\Omega^{\uparrow})$ from pixel ($i = i' - \Delta i$, $j = j' - \Delta j$) on top of (BA) along the upward direction $\Omega^{\uparrow}$.

Upward flux at sensor level: "Upward flux from BA" x "Transfer Functions $TF_{BA-Sensor}(\Delta i,\Delta j,\Omega^{\uparrow},\Omega'^{\uparrow})$"

$$W_{Sensor}\left(i', j', \Omega'^{\uparrow}\right) = \sum_i \sum_j \sum_{\Omega^{\uparrow}} W_{BOA}\left(i, j, \Omega^{\uparrow}\right).TF_{BOA,Sensor}\left(\Delta i, \Delta j, \Omega^{\uparrow}, \Omega'^{\uparrow}\right)$$

Energy absorbed in atmosphere layer n.

$$W_{FL}^{abs}(n) = \sum_i \sum_j \sum W_{BOA}\left(i, j, \Omega^{\uparrow}\right).TF_{FL}\left(n, \Omega^{\uparrow}\right) \text{ where FL} = \text{MA or HA.}$$

3.4. Automatic computation of DART atmosphere vertical geometry

The atmosphere geometry can be simulated more or less accurately by varying its parameters:

- number of layers $N_{layers,HA}$ of the HA atmosphere,
- numbers of layers $N_{layers,MA}$ and horizontal cells $N_{horizontal\ cells,MA}$ in the MA atmosphere, and
- altitude h_{FLMA} of the interface between HA and MA.

This flexibility allows us to obtain the best trade-off "Computer time–R.T. modeling accuracy". We developed a method that determines automatically the so-called optimal geometry (i.e., $N_{layers,HA}$, $N_{layers,MA}$, h_{FLMA}) because it is not intuitive. For that, accuracy criteria are applied to atmosphere TOA radiance $L_{atm,TOA}$ (i.e., remote sensing products) and BOA radiance $L_{atm,BOA}$. (i.e., radiative budget products).

DART simulates exactly the direct radiance values $L_{direct,atm,TOA}$ and $L_{direct,atm,BOA}$ because it uses direct transmittance values that are assumed to be exact. It simulates also exactly TOA and BOA 1st order (i.e., single scattering and/or thermal emission) atmosphere radiance values $L_{1,atm,TOA}$ and $L_{1,atm,BOA}$ because it uses scattering points M_s instead of cell centers. Multiple scattering modeling is the only source of inaccuracy for simulating $L_{atm,TOA}$ and $L_{atm,BOA}$. It cannot use points M_s because they are specifically computed for the sun direction. Instead, it uses the cell/layer centers as the origin of scattering. In this context, the atmosphere geometry (i.e., $N_{layers,HA}$, $N_{layers,MA}$, h_{FLMA}) plays an important role. For instance, large $N_{layers,HA}$ and $N_{layers,MA}$ numbers lead to accurate results, but with large computer times. Thus, it is useful to determine the so-called optimal atmosphere geometry that gives $L_{atm,TOA}$ and $L_{atm,BOA}$ values with pre-defined relative accuracy levels ε_{TOA} and ε_{BOA}. A difficulty comes from the fact that there are no exact analytical expressions of $L_{atm,TOA}$ and $L_{atm,BOA}$ due do multiple scattering. On the other hand, there

are analytical expressions of $L_{1,atm,TOA}$ and $L_{1,atm,BOA}$ due to single scattering, with cell centers as the origin of scattering. With the hypothesis that the accuracy of $L_{atm,TOA}$ and $L_{atm,BOA}$ due do multiple scattering has the same order of magnitude as the accuracy of $L_{1,atm,TOA}$ and $L_{1,atm,BOA}$ if both of them are computed with cell centers as the origin of scattering, the optimal atmosphere geometry is defined by the constraint: "atmosphere single scattering simulation, with cell centers as the origin of scattering, must lead to 1st order atmosphere radiance $L_{1,atm,TOA}$ and $L_{1,atm,BOA}$ values with relative accuracy levels ε_{TOA} and ε_{BOA}". Here, $L_{1,atm,TOA}$ is computed for a TOA downward irradiance, and $L_{1,atm,BOA}$ is computed for a BOA upward irradiance. The approach that computes automatically the atmosphere geometry is presented below. It takes into account the fact that the atmosphere is made of 2 layers (i.e., HA and MA). Optical depths that are mentioned in this presentation are for scattering phenomena only.

Let $\Omega_s(\theta_s,\phi_s)$ be an incident direction and $\Omega_v(\theta_v,\phi_v)$ a backscattering direction, with θ and ϕ the zenith and azimuth angles. Thus, we have either $\mu_s = \cos\theta_s < 0$ and $\mu_v = \cos\theta_v > 0$, for a downward incident direction and an upward scattered direction, or $\mu_s = \cos\theta_s > 0$ and $\mu_v = \cos\theta_v < 0$, for an upward incident direction and a downward scattered direction. We consider an atmosphere layer with an optical depth $\Delta\tau$, a phase function $\frac{P(\Omega_s,\Omega_v)}{4\pi}$ and a scattering albedo ω, with an incident irradiance $E_s.\mu_s$ along direction Ω_s. Its 1st order reflected radiance is:

$$L^{exact}_{1,atm,TOA}(\Omega_s,\Omega_v) = E_s.\frac{|\mu_s|}{|\mu_v|-|\mu_s|}.\left[1-\exp\left(-\left(\frac{\Delta\tau}{|\mu_s|}-\frac{\Delta\tau}{|\mu_v|}\right)\right)\right].\frac{P(\Omega_s,\Omega_v)}{4\pi}.\omega$$

$L^{exact}_{1,atm}(\Omega_s,\Omega_v)$ varies with the optical depth and the incident Ω_s and scattering Ω_v directions. The impact of optical depth depends on the Ω_s and Ω_v directions. Here, one assumes that the mean value of this impact is equal to its value for the intermediate directions Ω_s and Ω_v that have a $\frac{\pi}{3}$ off-nadir angle (i.e., $|\mu_s| = |\mu_v| = 0.5$). Thus, $L^{exact}_{1,atm,BOA}(\Omega_s,\Omega_v)$ is assumed to be proportional to $[1 - e^{-4\Delta\tau}]$.

The horizontal distribution of the radiation $E_{backscattered,atm}(x,y)$ that is backscattered by the atmosphere towards the Earth (i.e., "Atmosphere–Earth" radiative coupling) can be simulated by the MA atmosphere only. Indeed, the HA atmosphere cannot simulate horizontal variations because it is made of layers only, conversely to the MA atmosphere where each layer can contain $N_{horizontal\ cells,MA}$ cells. Thus, in order to simulate accurately the horizontal distribution of $E_{backscattered,atm}(x,y)$, the radiation $E_{backscattered,MA}$ that is backscattered by the MA atmosphere towards the Earth must be an important fraction (e.g., 50%) of $E_{backscattered,atm}$. If we call γ this fraction, we must have:

$$1-e^{-4\Delta\tau_{MA}} = \gamma\left(1-e^{-4\Delta\tau_{atm}}\right)$$

where $\Delta\tau_{atm}$ is the total atmosphere optical depth and $\Delta\tau_{MA}$ the MA atmosphere optical depth.

It implies that the optical depth of MA must be: $\Delta\tau_{MA} = -\frac{1}{4}.\ln\left[1-\gamma\left(1-e^{-4\Delta\tau_{atm}}\right)\right]$

Here, for an exponential atmosphere with a height factor H, we have: $\Delta\tau_{MA} = \Delta\tau_{atm}\left(1-e^{-\frac{h_{FLMA}}{H}}\right)$

Thus: $h_{FLMA} = -H.\ln\left(1-\frac{\Delta\tau_{MA}}{\Delta\tau_{atm}}\right)$ with $h_{FLMA} \in [0.1\ km–90\ km]$.

Once the h_{FLHA} altitude is defined, the procedure computes the terms $N_{layers,HA}$ and $N_{layers,MA}$ that lead to relative errors less than the user defined ε_{TOA} and ε_{BOA} values on the atmosphere 1st order TOA radiance $L_{1,atm,TOA}{}^{cell\ centre}(\Omega_s,\Omega_v)$ and BOA radiance $L^{cell\ centre}_{1,atm,BOA}(\Omega_s,\Omega_v)$ that DART would give. The expression of the error on the upward radiance $L_{1,atm,TOA}{}^{cell\ centre}(\Omega_s,\Omega_v)$ is given below for an exponential atmosphere, with N_{layers} layers, in the presence of a direct downward irradiance $E_s.\mu_s$ along direction Ω_s. Any atmosphere layer n is characterized by its own optical depth $\Delta\tau_n$ and its optical depth τ_n relative to the top of the atmosphere. With atmosphere components characterized by a single scattering ω and a phase function $\frac{P(\Omega_s,\Omega_v)}{4\pi}$, we have:

$$L^{cell\ centre}_{1,atm,TOA}(\Omega_s,\Omega_v) = E_s.\frac{|\mu_s|}{\mu_v}.\frac{P(\Omega_s,\Omega_v)}{4\pi}.\omega.\sum_{n=1}^{N_{layers}}\left[\left(1-e^{\frac{\Delta\tau_n}{\mu_s}}\right).e^{\frac{-\Delta\tau_n}{2\mu_v}}.e^{\left(\frac{\tau_n}{\mu_s}-\frac{\tau_n}{\mu_v}\right)}\right]$$
$$\text{with } \tau_n = \tau_{atm}.e^{-\frac{n\Delta h}{H}} \text{ and } \Delta\tau_n = \tau_{atm}.\left(e^{-\frac{(n-1)\Delta h}{H}}-e^{-\frac{n\Delta h}{H}}\right)$$

$\left(1-e^{\frac{\Delta\tau_n}{\mu_s}}\right)$ is the fraction of the downward incident irradiance that is intercepted by layer n, $e^{\frac{-\Delta\tau_n}{2\mu_v}}$ is layer n transmittance for the 1st order scattered radiation and $e^{\left(\frac{\tau_n}{\mu_s}-\frac{\tau_n}{\mu_v}\right)}$ is the transmittance from TOA down to layer n from layer n up to TOA.

Thus, the relative error on $L^{cell\ centre}_{1,atm,TOA}(\Omega_s,\Omega_v)$ is:

$$\varepsilon\left(L^{cell\ centre}_{1,atm,TOA}(\Omega_s,\Omega_v)\right) = \frac{\left|L^{cell\ centre}_{1,atm,TOA}(\Omega_s,\Omega_v)-L^{exact}_{1,atm,TOA}(\Omega_s,\Omega_v)\right|}{L^{exact}_{1,atm,TOA}(\Omega_s,\Omega_v)}.$$

Similarly:

$$\varepsilon\left(L^{cell\ centre}_{1,atm,BOA}(\Omega_s,\Omega_v)\right) = \frac{\left|L^{cell\ centre}_{1,atm,TOA}(\Omega_s,\Omega_v)-L^{exact}_{1,atm,BOA}(\Omega_s,\Omega_v)\right|}{L^{exact}_{1,atm,BOA}(\Omega_s,\Omega_v)}.$$

1st order atmosphere radiance (i.e., $L_{1,atm,TOA}$ and $L_{1,atm,BOA}$) at TOA and BOA levels is analytically computed as the sum of 2 radiance components from the HA and MA atmospheres. A 2 step approach is used.

1) Step a: $L_{1,atm,TOA}$ is computed for a downward incident direction ($\mu_s < 0$) and an upward scattered direction ($\mu_v > 0$). Two configurations are considered:
   - $L_{1,atm,TOA} = L^{cell\ centre}_{1,HA,TOA} + L^{exact}_{1,MA,TOA}$
     $L^{cell\ centre}_{1,HA,TOA}$ is computed with HA made of $N_{layers,HA,a}$ layers. $L^{exact}_{1,MA,TOA}$ is exactly computed as an analytic integral. $N_{layers,HA,a}$ is iteratively computed as the smaller number for which the error on 1st order radiance verifies: $\varepsilon\left(L^{cell\ centre}_{1,HA,TOA}\right) < \varepsilon_{TOA}\frac{s\left(L^{exact}_{1,HA,TOA}\right)}{s\left(L^{exact}_{1,atm,TOA}\right)}$. Computer time is reduced by using a unique incident direction Ω_{so} and a unique scattering direction Ω_v that are intermediate directions with $\theta_{so} = \frac{2\pi}{3}$ and $\theta_{vo} = \frac{\pi}{3}$ (i.e., $|\mu_{so}| = \mu_{vo} = 0.5$). Thus, $N_{layers,HA,a}$ must be such that:

$$\varepsilon\left(L^{cell\ centre}_{1,HA,TOA}(\Omega_{vo})\right) < \varepsilon_{TOA}\frac{1-e^{\left(\frac{\Delta\tau_{HA}}{\mu_{so}}-\frac{\Delta\tau_{HA}}{\mu_{vo}}\right)}}{1-e^{\left(\frac{\Delta\tau_{atm}}{\mu_{so}}-\frac{\Delta\tau_{atm}}{\mu_{vo}}\right)}}$$

   - $L_{1,atm,BOA} = L^{exact}_{1,HA,TOA} + L^{cell\ centre}_{1,MA,TOA}$
     $L^{exact}_{1,HA,TOA}$ is exactly computed as an analytic integral, and $L^{cell\ centre}_{1,MA,TOA}$ is computed with MA made of $N_{layers,MA,a}$ layers. The number $N_{layers,MA,a}$ of MA layers must be such that:

$$\varepsilon\left(L^{cell\ centre}_{1,MA,TOA}(\Omega_{vo})\right) < \varepsilon_{TOA}\frac{1-e^{\left(\frac{\Delta\tau_{MA}}{\mu_{so}}-\frac{\Delta\tau_{MA}}{\mu_{vo}}\right)}}{1-e^{\left(\frac{\Delta\tau_{atm}}{\mu_{so}}-\frac{\Delta\tau_{atm}}{\mu_{vo}}\right)}}.e^{\left(\frac{\Delta\tau_{HA}}{\mu_{so}}-\frac{\Delta\tau_{HA}}{\mu_{vo}}\right)}$$

2) Step b: $L_{1,atm,BOA}$ is computed for an upward incident direction ($\mu_s > 0$) and a downward scattered direction ($\mu_v < 0$). Two configurations are considered:
   - $L_{1,atm,BOA} = L^{exact}_{1,HA,BOA} + L^{cell\ centre}_{1,MA,BOA} L^{exact}_{1,HA,BOA}$ is exactly computed as an analytic integral and $L^{cell\ centre}_{1,MA,BOA}$ is computed with "MA made of $N_{layers,MA,b}$ layers". The constraint on the accuracy of $L^{cell\ centre}_{1,MA,BOA}$ is verified if $N_{layers,MA,b}$ is such that:

$$\varepsilon\left(L^{cell\ centre}_{1,MA,BOA}(\Omega_{vo})\right) < \varepsilon_{BOA} \frac{1-e^{\left(\frac{\Delta\tau_{MA}}{\mu_{so}}+\frac{\Delta\tau_{MA}}{\mu_{vo}}\right)}}{1-e^{\left(\frac{\Delta\tau_{atm}}{\mu_{so}}+\frac{\Delta\tau_{atm}}{\mu_{vo}}\right)}}$$

   - $L_{1,atm,BOA} = L^{cell\ centre}_{1,HA,BOA} + L^{exact}_{1,MA,BOA}$
   $L^{cell\ centre}_{1,HA,BOA}$ is computed with HA made of $N_{layers,HA,b}$ layers and $L_{1,MA,BOA}{}^{exact}$ is exactly computed as an analytic integral. The constraint on the accuracy of $L^{cell\ centre}_{1,HA,BOA}$ is verified if $N_{layers,HA,b}$ is such that:

$$\varepsilon\left(L^{cell\ centre}_{1,HA,BOA}(\Omega_{vo})\right) < \varepsilon_{BOA} \frac{1-e^{\left(\frac{\Delta\tau_{HA}}{\mu_{so}}-\frac{\Delta\tau_{HA}}{\mu_{vo}}\right)}}{1-e^{\left(\frac{\Delta\tau_{atm}}{\mu_{so}}-\frac{\Delta\tau_{atm}}{\mu_{vo}}\right)}} . e^{\left(\frac{\Delta\tau_{MA}}{\mu_{so}}-\frac{\Delta\tau_{MA}}{\mu_{vo}}\right)}.$$

Finally, we get: $N_{layers,HA} = Max(N_{layers,HA,a}, N_{layers,HA,b})$ and $N_{layers,MA} = Max(N_{layers,MA,a}, N_{layers,MA,b})$.

The procedure that simulates automatically the atmosphere geometry uses an iterative approach with preset conditions for stopping it:

- $N_{layers} \leq 100$, with $N_{layers} = N_{MA,layers}$ or $N_{layers} = N_{HA,layers}$
- $|L^{cell\ centre}_{1,atm,\Upsilon}(\Omega_{vo}) - L^{exact}_{1,atm,\Upsilon}(\Omega_{vo})| \lesssim 5\ 10^{-7}$ for a unit irradiance value, with Υ = BOA or TOA.
- $\frac{|L^{cell\ centre}_{1,X,\Upsilon}(\Omega_{vo}) - L^{exact}_{1,X,\Upsilon}(\Omega_{vo})|}{L^{exact}_{1,X,\Upsilon}(\Omega_{vo})} \lesssim Max\left(10^{-3}; \varepsilon_0\right)$ with ε_o the user specified error, X = MA or HA and Y = BOA or TOA.
  with N_{layers}(iteration i + 1) = N_{layers}(iteration i) + 1.
- $\left\{\frac{|L^{cell\ centre}_{1,atm,\Upsilon}(\Omega_{vo}) - L^{exact}_{1,atm,\Upsilon}(\Omega_{vo})|}{L^{exact}_{1,atm,\Upsilon}(\Omega_{vo})}\right\}_{iteration\ i+1} - \left\{\frac{|L^{cell\ centre}_{1,atm,\Upsilon}(\Omega_{vo}) - L^{exact}_{1,atm,\Upsilon}(\Omega_{vo})|}{L^{exact}_{1,atm,\Upsilon}(\Omega_{vo})}\right\}_{iteration\ i} \lesssim 10^{-4}$

Actually, in addition to this automatic computation of the optimal atmosphere geometry, the atmosphere geometry can be also simulated with the 2 following approaches:

- "Fast" approach: the whole atmosphere is a simple superimposition of layers (i.e., $N_{horizontal\ cells,MA} = 1$), the maximum number of layers of MA and HA is 30, $\gamma = 95\%$ and $\varepsilon_o = 20\%$.
- "Manual approach": the user defines all geometry parameters $N_{layers,HA}$, $N_{layers,MA}$, $N_{horizontal\ cells,MA}$, h_{FLMA},…

This procedure can be applied to all possible DART configurations. Two examples are given below:

- Simulation of N_λ (e.g., 10^2) spectral bands, either all together (one simulation with N_λ bands) or sequentially (N_λ simulation with one band). For a sequential modeling, the atmosphere geometry is computed independently for each spectral band. For a parallel modeling, a single atmosphere geometry is computed, using the band for which the atmosphere optical depth is larger.
- Spectral band where there is thermal emission only, without any sun irradiance. The procedure determines the so-called optimal geometry that leads to an accurate simulation of scattering mechanisms.

Table 3 shows atmosphere parameters (i.e., $N_{layers,HA}$, $N_{layers,MA}$, h_{FLMA}) and the associated computer time for simulating the atmosphere geometry with the fast mode and the automatic mode, with 3 relative error thresholds ε on TOA and BOA radiance values. Atmosphere optical depths are $\Delta\tau_{scat} = 0.8$ and $\Delta\tau_{abs} = 0.29$. As expected, the number of layers increases if ε decreases. The fast mode leads to the simpler atmosphere geometry with the smaller computer time. The associated relative error is less than 0.5%, which is quite acceptable for many applications. It is interesting to note that the atmosphere discretization remains the same if ε becomes smaller than 0.01.

Table 3
Automatically computed atmosphere parameters (i.e., $N_{layers,HA}$, $N_{layers,MA}$, h_{FLMA}) from the fast mode and the automatic mode with 3 radiance relative error thresholds, and associated computer times with a 2.5 GHz computer. Parameters: $\Delta\tau_{scat} = 0.8$, $\Delta\tau_{abs} = 0.29$, $\gamma = 95\%$, $\theta_s = 30°$, TOA vertical solar constant $E_{TOA} = 1000$ W/m²/μm and $\rho_{ground} = 1$.

Approach	h_{FLMA}	$N_{layers,MA}$	$N_{layers,HA}$	Δt [s]	TOA exitance [W/m²/μm]
Fast	8.537	4	11	1	355.23
Automatic (ε = 0.2%)	8.533	9	35	4	355.48
Automatic (ε = 0.1%)	8.529	13	48	6	355.51
Automatic (ε ≤ 0.01%)	8.533	27	61	8	355.53

3.5. Simulation products

DART simulates a large number of remote sensing products (e.g., images of reflectance, brightness temperature, radiance, irradiance, exitance and albedo values) for the BOA, Sensor and TOA altitude levels. It computes also several Earth and Atmosphere radiative budget products (e.g., profiles and 3D distributions of the energy that is intercepted, scattered, emitted and absorbed). DART simulated images are georeferenced and can be ortho-projected using a Digital Elevation Model (DEM). Hereafter, the remote sensing products are noted X. Fig. 6 shows 2 types of TOA and BOA atmosphere products:

- TOA: upward 1st scattering order $X_{1,atm,TOA}$ (Fig. 6a) and total $X_{atm,TOA}$ (Fig. 6b). $X_{atm,TOA}$ includes single and multiple scattering, and thermal emission, without any Earth influence.
- BOA: upward and downward products: without $X^{no\ coupling}_{atm,BOA}$ (Fig. 6c) and with $X_{atm,BOA}$ (Fig. 6d) "Earth–Atmosphere" coupling.

Components of remote sensing signals and radiative budgets with/without atmosphere scattering and with/without Earth–Atmosphere radiative coupling can also be computed. For that, DART simulates 3 types of BOA downward fluxes and 3 types of upward fluxes for the BOA, Sensor and TOA levels. This leads to 9 radiative configurations, as explained below. As for the BOA level, the direct and hemispheric (diffuse) downward fluxes at the Sensor level are simulated for computing reflectance values at the Sensor level. The abovementioned radiative components are noted $X_{i-j,level}$ where index "i" is downward fluxes at BOA and Sensor levels and index "j" is for upward fluxes at Sensor and TOA levels (Fig. 7):

- i = d (direct): downward fluxes that come directly from the sun or from atmosphere thermal emission, without any atmosphere scattering.
- i = h (hemispheric): downward fluxes that come from the sun or the atmosphere thermal emission after some scattering by the atmosphere.
- i = t (total): downward fluxes that have been or not scattered by the atmosphere. This case includes a configuration that is not taken into account by the configuration "i = d + h": the "Earth–Atmosphere" coupling associated to the direct irradiance of Earth surfaces.
- j = d (direct): upward fluxes that come directly from the Earth surface, whatever the type (i.e., direct or hemispheric) of BOA downward flux, or directly from the atmosphere thermal emission, without any atmosphere scattering.
- j = h (hemispheric): upward fluxes that have been scattered by the atmosphere.
- j = t (total): upward fluxes that have been or not scattered by the atmosphere.

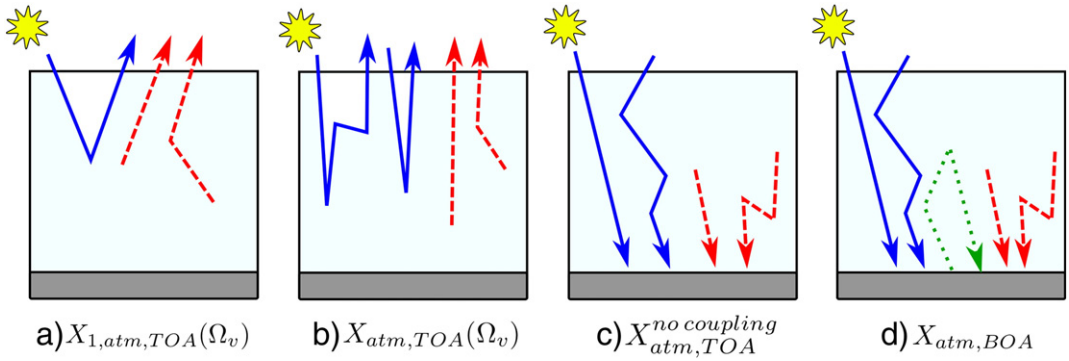

Fig. 6. Atmosphere products (X = reflectance, radiance, brightness temperature). Radiation sources are the sun (blue) and the Earth and the atmosphere (red). TOA: a) Single scattering. b) Total (scattering + thermal emission). BOA: c) Total without No "Earth–Atmosphere" coupling. d) Total.

Four examples of components $X_{i-j,TOA}(\Omega_v)$ at TOA level associated to DART mode (R) are given below:

- $X_{d-d,TOA}(\Omega_v)$: Earth direct irradiance (i.e., no atmosphere scattering on the way "Sun–Earth") and direct TOA irradiance from the Earth (i.e., no atmosphere scattering on the way "Earth–TOA").
- $X_{d-h,TOA}(\Omega_v)$: Earth direct irradiance (i.e., no scattering on the way "Sun–Earth") and hemispheric TOA irradiance from the Earth (i.e., scattering and/or thermal emission on the way "Earth–TOA").
- $X_{h-d,TOA}(\Omega_v)$: Earth hemispheric irradiance (i.e., atmosphere scattering on the way "Sun–Earth") and TOA direct irradiance from the Earth (i.e., no atmosphere scattering on the way "Earth–TOA").
- $X_{h-h,TOA}(\Omega_v)$: Earth hemispheric irradiance (i.e., scattering on the way "Sun_Earth") and TOA hemispheric irradiance from the Earth (i.e., scattering/thermal emission on the way "Earth_TOA").

The X_{i-j} components are related by the following expressions:

$$X_{d\text{-}t,TOA}(\Omega_v) = X_{d\text{-}d,toTOA}(\Omega_v) + X_{d\text{-}h,TOA}(\Omega_v) + X_{d\text{-coupling-}h,TOA}(\Omega_v) \text{ and } X_{h\text{-}t,TOA}(\Omega_v) = X_{h\text{-}d,TOA}(\Omega_v) + X_{h\text{-}h,TOA}(\Omega_v)$$

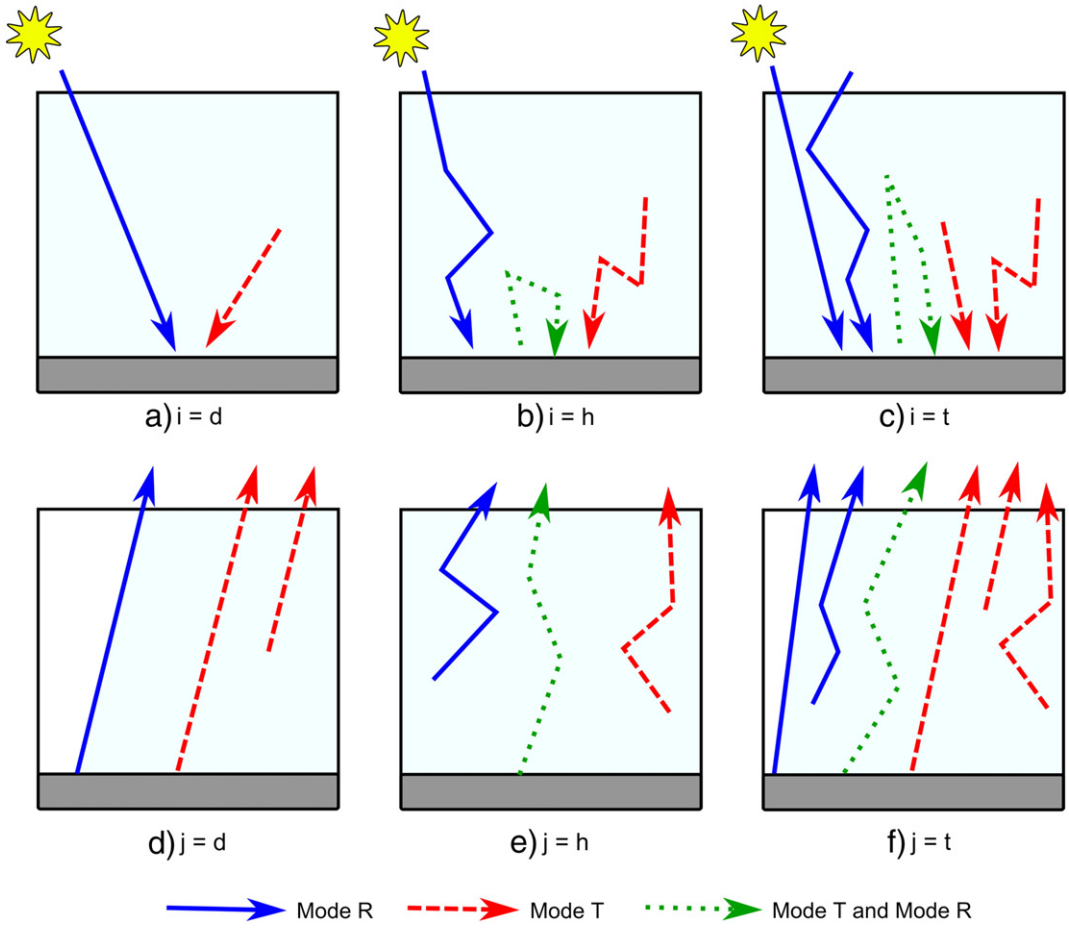

Fig. 7. The 3 downward fluxes "i" (a: Direct d, b: Hemispheric h, c: Total t) and the 3 upward fluxes "j" (d: Direct d, e: Hemispheric h, f: Total t) for remote sensing components X_{i-j}. Blue color is for sun flux, direct and scattered by the atmosphere. Red color is for Earth/Atmosphere thermal flux. Green color is for Earth scattered flux, from hemispheric sun and Earth/Atmosphere thermal fluxes (solid line), or from direct sun and atmosphere thermal fluxes (dotted line).

The term $X_{d-coupling-h}(\Omega_v)$ stands for the "Earth–Atmosphere" coupling due to the Earth direct irradiance, from the sun and/or atmosphere thermal emission.

The separation between direct and hemispheric radiance values is very useful for studying directional effects (Vermote et al., 1997; Verhoef & Bach, 2003), topographic effects (Hay & Davies, 1978; Ricchiazzi et al., 1998) and adjacency effects (Dave, 1980; Mekler and Kaufman, 1982; Lee and Kaufman, 1986; Vermote et al., 1997).

4. Tests of validity

This chapter illustrates how the new atmosphere R.T. module improves DART products.

4.1. Beer law adaptation

To simulate the atmosphere R.T. with the Beer law, even in spectral domains with strong absorption variations where this law is not valid, DART uses pre-computed transmittance values $T^{\updownarrow}_{gas,abs}(\lambda)$ that take into account this non-Beer law behavior of the atmosphere R.T. These transmittance values are stored in the DART database. $T^{\updownarrow}_{gas,abs}(\lambda)$ is the spectral coupled direct path transmittance, at a 1 cm^{-1} resolution for a pure gaseous atmosphere. In addition, DART uses the downward direct transmittance $T^{\downarrow}_{gas,abs}(\lambda)$. As already mentioned, $T^{\updownarrow}_{gas,abs}(\lambda)$ and $T^{\downarrow}_{gas,abs}(\lambda)$ are pre-computed with the MODTRAN model (Berk & Bernstein, 1999) for major standard atmosphere models and for nadir sun and view directions. It explains that DART and MODTRAN TOA simulations are nearly equal for sun and view directions close to nadir.

Fig. 8 compares MODTRAN TOA reflectance, from 0.32 μm to 2.3 μm, to DART TOA reflectance that is simulated without and with the use of $T^{\updownarrow}_{gas,abs}(\lambda)$. All scattering orders are simulated. Here, one considers a US-Standard atmosphere with nadir sun and view directions. MODTRAN simulations were conducted with the DISORT algorithm, using 8 iterations. DART reflectance is usually very close to MODTRAN reflectance.

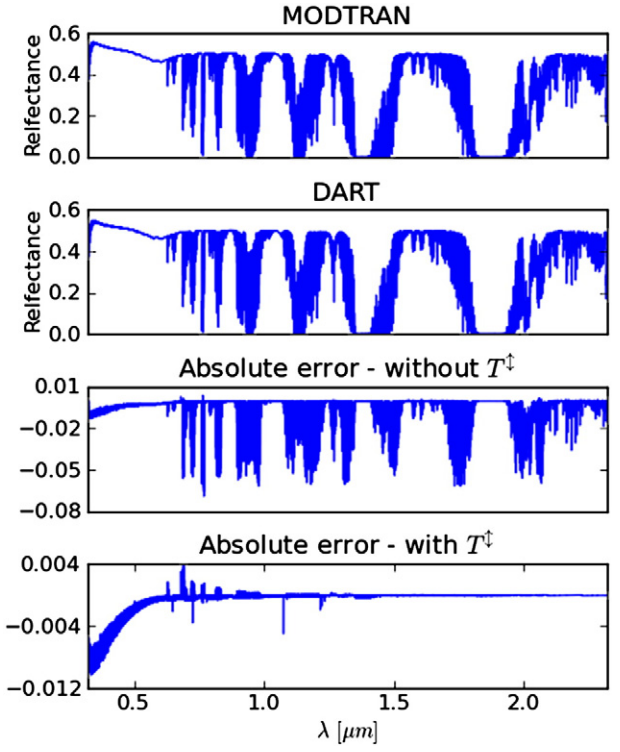

Fig. 8. DART and MODTRAN TOA reflectance spectra at 1 cm^{-1} resolution. From top to bottom: a) MODTRAN reflectance. b) DART reflectance. c) Absolute error "MODTRAN–DART" without Beer law adaptation. d) Absolute error MODTRAN–DART with Beer law adaptation. US-Standard atmosphere. $\rho_{ground} = 0.5$, $\theta_s = 180°$. $\theta_v = 0°$.

However, its absolute error can be as large as 0.05 if the atmosphere R.T. is simulated with Beer law using the transmittance $T^{\downarrow}_{gas,abs}(\lambda)$ and not $T^{\uparrow}_{gas,abs}(\lambda)$. Use of $T^{\downarrow}_{gas,abs}(\lambda)$ improves a lot results, with an absolute error that is less than 0.004 for all wavelengths larger than 0.4 μm. It can be noted that differences increase for wavelengths smaller than 0.4 μm. We assume that these differences are due to multiple scattering, because MODTRAN and DART do not use the same approach for modeling multiple scattering. Maximal error reaches 0.0104 (i.e., 1.8% in relative) at 0.32 μm. The above results justify the Beer's law adaptation by DART: simulation of the atmosphere R.T. with transmittance values that account for the non-Beer's law behavior of atmosphere R.T.

It is interesting to note that without the Beer law adaptation, DART and MODTRAN reflectance differences increase if bandwidths Δλ increase. Indeed, the approximation $T^{\uparrow}_{gas,abs}(\lambda) = [T^{\downarrow}_{gas,abs}(\lambda)]^2$ is less and less valid if Δλ increases, at least in spectral domains where optical properties strongly vary. This is illustrated by Fig. 9. It shows DART reflectance values simulated without and with the use of $T^{\updownarrow}_{gas,abs}(\lambda)$, for bandwidths Δλ equal to 0, 0.01 μm and 0.1 μm. DART–MODTRAN differences without $T^{\updownarrow}_{gas,abs}(\lambda)$ increase a lot if Δλ increases. On the other hand, DART–MODTRAN differences remain nearly equal to zero if Δλ increases with $T^{\updownarrow}_{gas,abs}(\lambda)$.

4.2. Use of points M_s as the origin of 1st order scattering

The use of points M_s as the origin of 1st order scattering (see Appendix A) is expected to lead to exact 1st order TOA reflectance values, whatever the number of layers used for simulating the atmosphere geometry. This is shown here, using the atmosphere analytic 1st order reflectance:

$$\rho^{analytic}_{1,atm,TOA}(\Omega_s,\Omega_v) = \frac{1}{\mu_v - \mu_s}\cdot\left[1 - e^{\left(\frac{\Delta\tau}{\mu_s} - \frac{\Delta\tau}{\mu_v}\right)}\right]\cdot\frac{P_R(\Omega_s,\Omega_v)}{4\pi}\cdot\omega$$

with $\frac{P_R(\Omega_s,\Omega_v)}{4\pi}$ the Rayleigh phase function (Chandrasekhar, 1960).

Fig. 10 shows the analytic reflectance $\rho^{analytic}_{1,atm,TOA}$ and 3 DART TOA first order reflectance products, as a function of the atmosphere optical depth, for a 30° sun off-nadir angle and a 40° view zenith angle in the solar plane and in the perpendicular plane. The 3 DART configurations are characterized by:

- M_s points are the origin of scattering and the atmosphere geometry is automatically computed.
- M_s points are the origin of scattering and the atmosphere geometry is simulated with 8 layers.
- Cell centers are the origin of scattering and the atmosphere geometry is simulated with 8 layers.

With the analytic reflectance $\rho^{analytic}_{1,atm,TOA}$ as a reference, Fig. 10 shows also the associated absolute and relative differences. As expected, the use of points M_s leads to exact results, even if the number of atmosphere layers is very small (e.g., 8 layers). On the other hand, R.T. simulation using cell centers instead of M_s points as scattering points leads to errors that increase with large atmosphere optical depths. For example, the relative error reaches 6% for an optical depth equal to 2.

Fig. 11 shows how DART 1st order reflectance varies with the view and sun zenith angles. The analytic expression of 1st order TOA reflectance is used as a reference. Similarly to the variation of TOA 1st order reflectance with the optical depth, the use of points M_s allows DART to simulate exact TOA 1st order reflectance. If these points are not used, differences with the analytical reflectance reach large values such as 10% with a 70° view zenith angle. This stresses the usefulness of the M_s points for simulating exactly 1st order reflectance.

4.3. DART convergence

DART accuracy depends on how the xyz coordinate and 4π direction spaces are discretized. A basic assumption is that DART simulation is

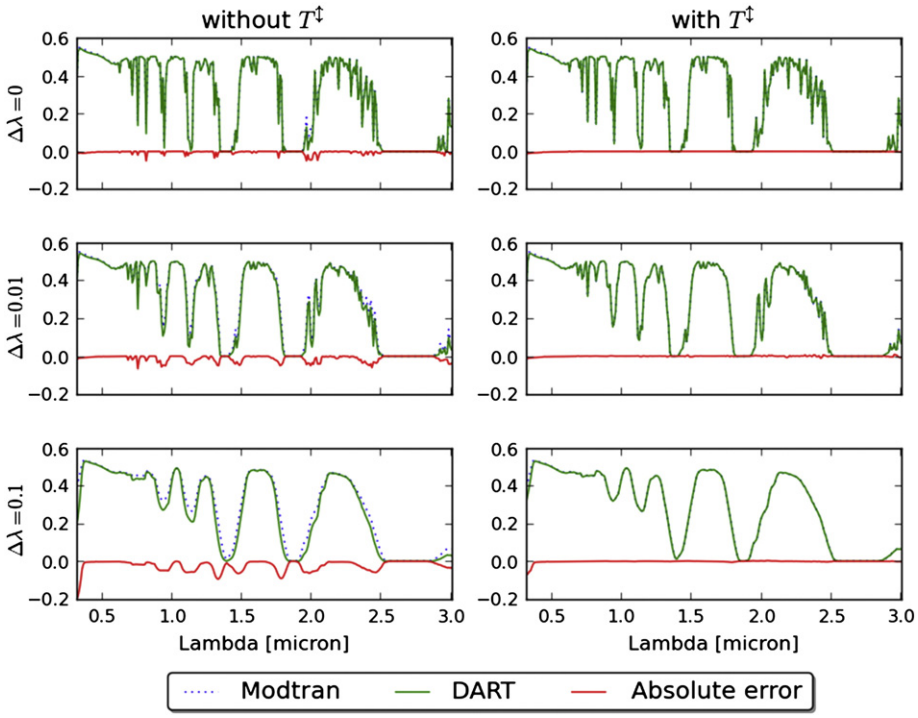

Fig. 9. DART (green) and MODTRAN (blue, dotted line) TOA reflectance with a 0.1 μm step, for 3 bandwidths (0, 0.01 μm, 0.1 μm), without (left)/with (right) spectral coupled direct path transmittance $T^{\updownarrow}_{gas,abs}(\lambda)$. Relative difference (red) increases with bandwidth if $T^{\updownarrow}_{gas,abs}(\lambda)$ is not used. $\rho_{ground} = 0.5$, $\theta_s = 180°$. $\theta_v = 0°$.

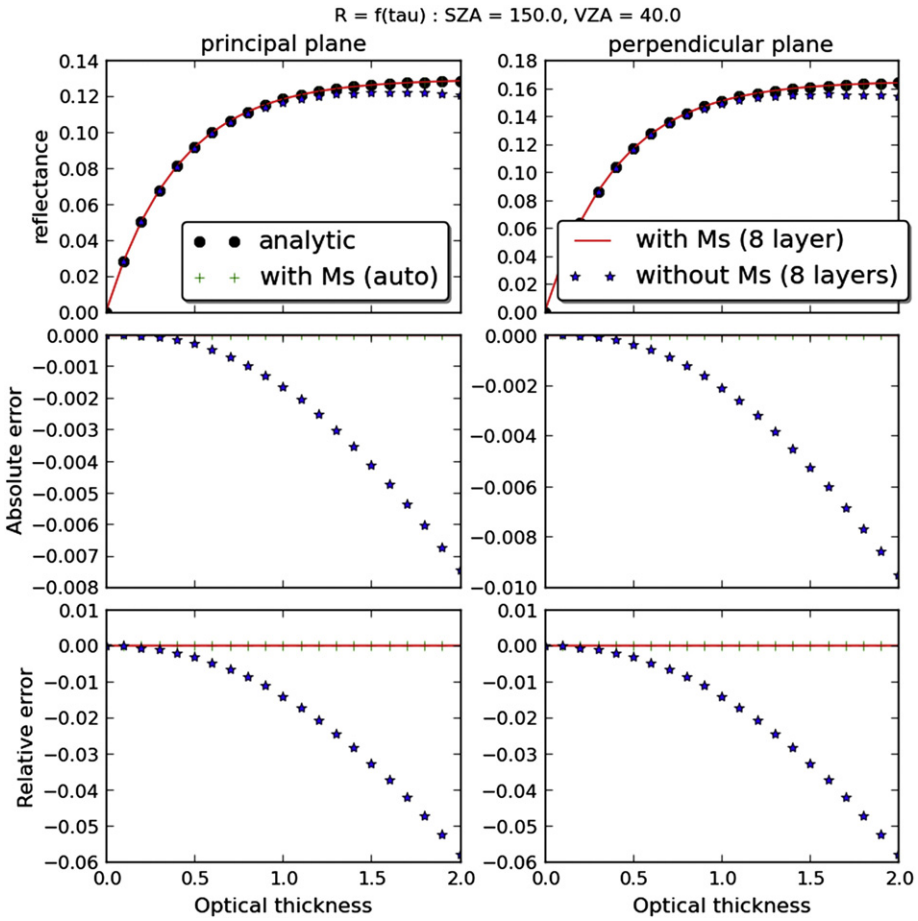

Fig. 10. DART and analytic atmosphere reflectance with variable optical depth. Reflectance (top), absolute (middle), and relative (bottom) errors. 30° sun off-nadir angle. 40° view zenith angle in the solar (left) and perpendicular (right) planes. 3 DART atmosphere configurations: "8 layers, no M_s", "8 layers, with M_s" and "automatic geometry, with M_s".

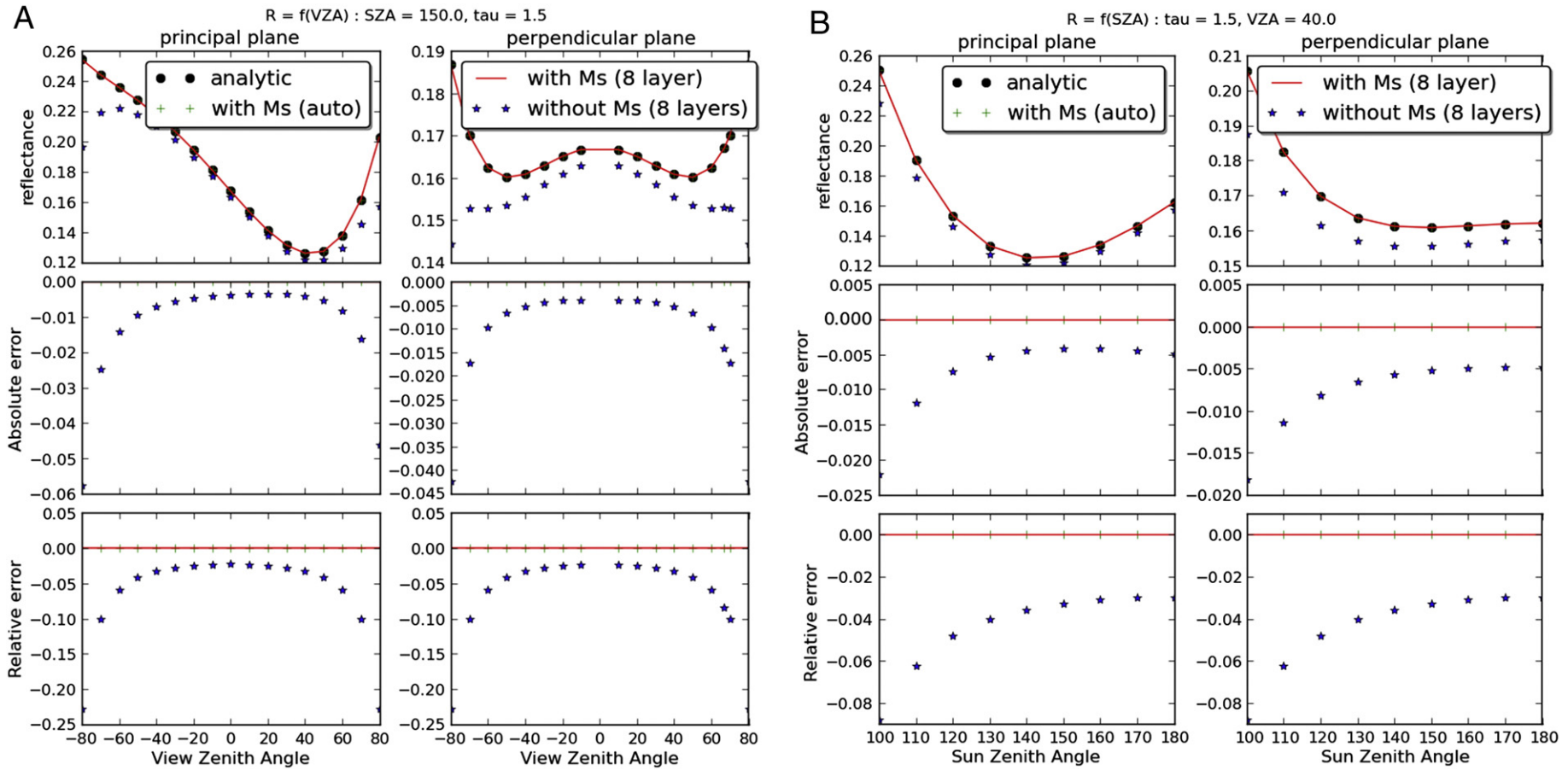

Fig. 11. DART and analytic atmosphere reflectance with variable sun and zenith angles. Reflectance (top), absolute (middle), and relative (bottom) errors. Solar (left) and perpendicular (right) planes, with 3 DART atmosphere configurations: "8 layers, no M_s", "8 layers, with M_s" and "automatic geometry, with M_s". Optical depth is 1.5. A) Variable view zenith angle. Sun zenith angle is 30°. B) Variable sun zenith angle. View zenith angle is 40°.

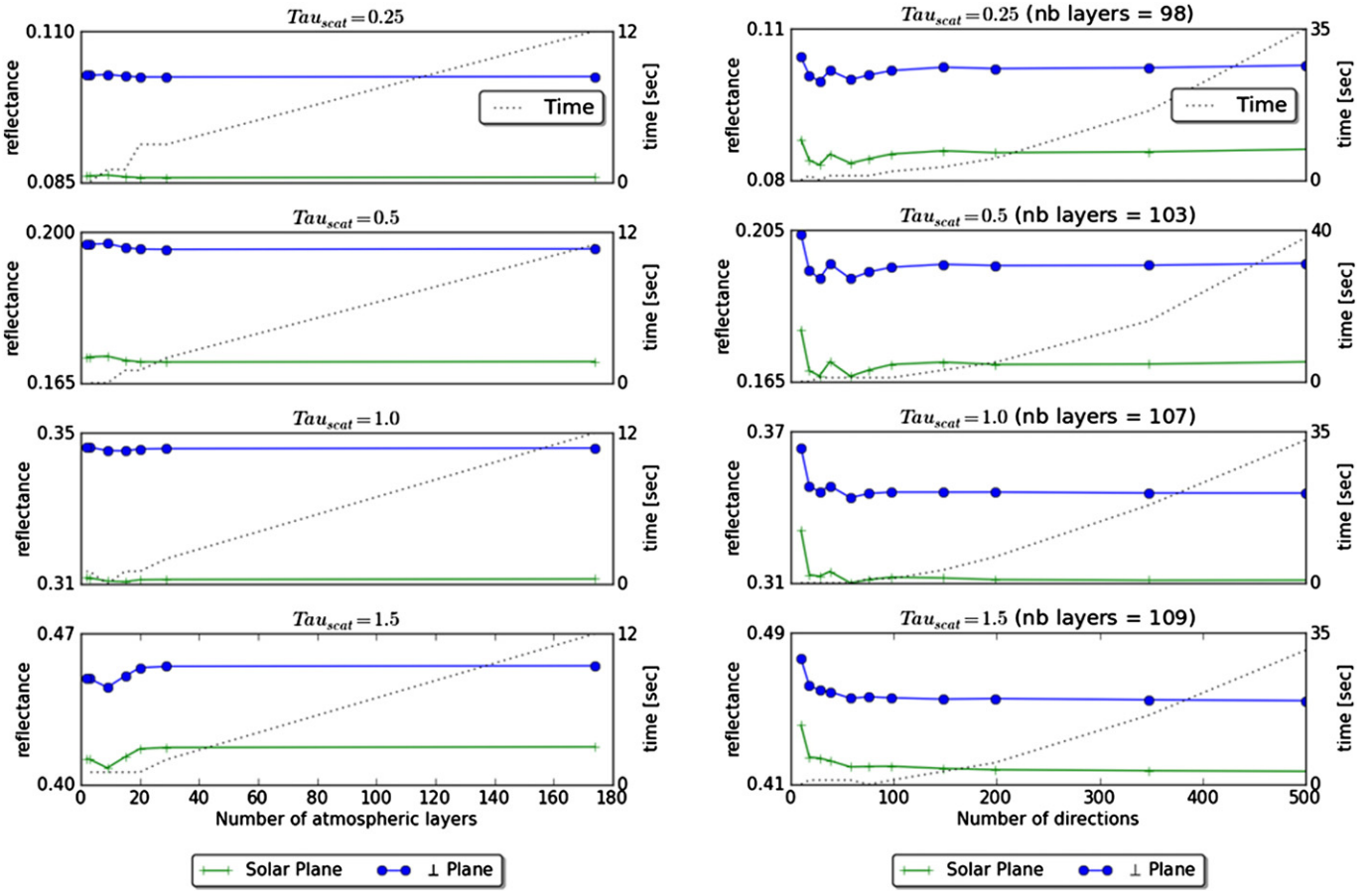

Fig. 12. DART reflectance of a non-absorbing gas atmosphere in the solar and perpendicular planes. a) Number of atmosphere layers from 1 up to 180, with 100 directions. b) Number of discrete directions from 2 to 500. Four atmosphere optical depths: 0.25, 0.5, 1, 1.5, with a number of atmosphere layers close to 100. Computer time is also shown (dotted line).

optimal if the sampling grid of these 2 spaces is infinitely small. Obviously, this is impossible because the numbers of cells and directions must be finite in order to be manageable, even if DART can handle very large numbers of cells and directions (e.g., 10^3 directions). Thus, the problem is to determine the xyz space and 4π space sampling grids that give the best trade-off in terms of simulation accuracy and computer time. Generally speaking, the sampling grid of the xyz space must be adapted to the dimensions of the scene elements that influence the scene radiative budget and/or its remote sensing images. As a rule of thumb, and in order to comply with the Nyquist–Shannon sampling theorem, the xyz sampling grid must be smaller than half the dimension of the smaller element that must be considered. In the case of the atmosphere, the sampling grid must be small enough for an accurate R.T. modeling, especially in presence of a heterogeneous Earth surface. The already presented automatic procedure computes the optimal atmosphere geometry.

Fig. 12 shows how DART reflectance varies with the number of atmosphere layers, from 1 up to 180 layers, and with the number of directions, from 2 up to 500 directions. Here, we consider a 30° sun zenith angle, a 40° view zenith angle in the solar and perpendicular planes, and a non-absorbing atmosphere with 4 optical depths (i.e., 0.25, 0.5, 1, and 1.5). In all cases, DART converges fast. For example, the simulation of TOA reflectance with 30–40 atmosphere layers is very close to the simulation

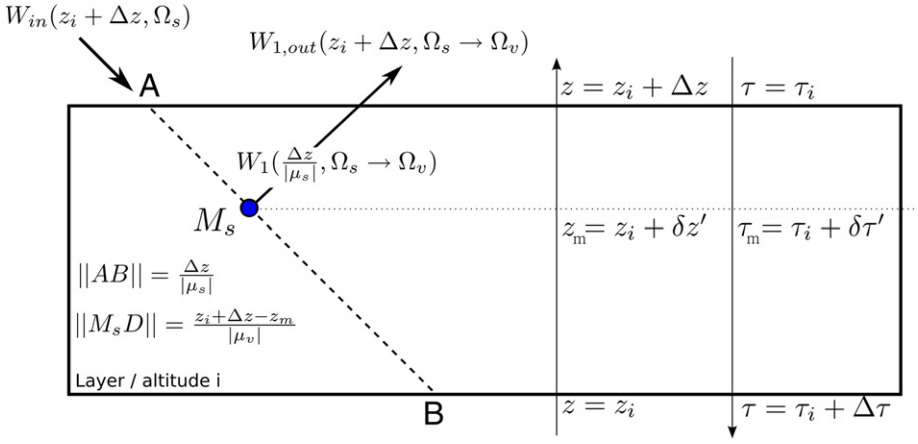

Fig. 13. Illustration of the calculation of the altitude of the 1st order scattering points M_s (Ω_v) in the DART atmosphere cells and layers.

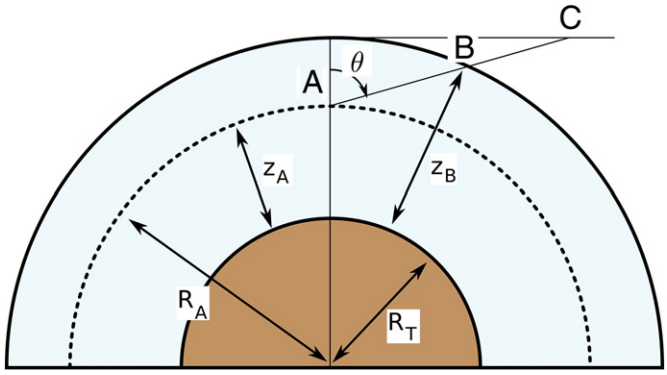

Fig. 14. Path AB along a direction with a θ zenith in a spherical atmosphere. Here, R_T is the Earth radius and R(z) is the radius of the sphere at the altitude z. $R_A(z) = R_t + z_A$.

with 180 layers; the relative difference is less than 10^{-4}. Thus, a number of 30–40 layers are usually large enough, whatever the atmosphere optical depth. The "optimal" number is given by the procedure that simulates automatically the atmosphere geometry. Similarly, TOA reflectance simulated with 100 discrete directions is very close to that simulated with 500 directions, whatever the atmosphere optical depth.

Reflectance in the solar plane is systematically smaller than in the perpendicular plane. Indeed, the phase angle is larger in the solar plane, which gives a small gas phase function value (i.e., Rayleigh phase function). Fig. 12 shows also computer time for an Intel 2.5 GHz processor. As expected, computer time increases when the numbers of atmosphere layers and directions increase.

The above results stress that for usual configurations of the "Earth–Atmosphere" system, DART reaches convergence with relatively small numbers of atmosphere layers (around 100) and discrete directions (around 100). This is very interesting in terms of computer time.

5. Concluding remarks

The atmosphere R.T. code presented in this paper transforms DART into an "Earth–Atmosphere" model that takes into account the scattering and absorption mechanisms of gasses and aerosols in a spherical "Earth–Atmosphere" system. Comparisons with MODTRAN4 model showed that DART leads to very comparable results with differences less than 0.004 for wavelengths larger than 0.4 μm. These excellent results are explained by the fact that the DART R.T. atmosphere module uses transmittance values that are pre-computed by the MODTRAN model for a number of major atmosphere models. The use of these transmittance values allows DART to simulate R.T. with Beer law, even in spectral domains with very strong spectral variations where the application of this law becomes less accurate. The major advantage of DART is to combine an accurate atmosphere R.T. modeling with a very accurate R.T. modeling of man-made and natural Earth scenes. As a result, it simulates accurately the radiative coupling of the "Earth–Atmosphere" system, with possibly complex and anisotropic Earth scenes.

Different modeling procedures were introduced for improving the atmosphere radiative transfer in the DART model. The approach was

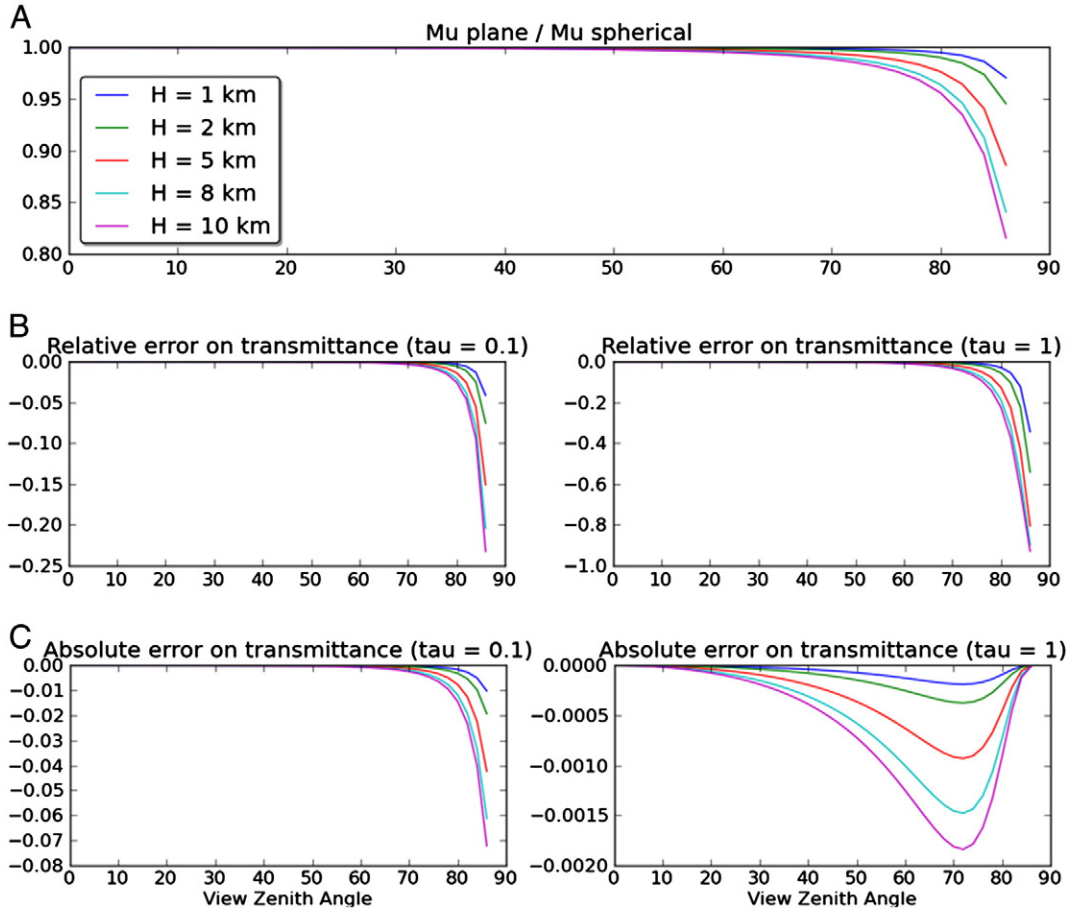

Fig. 15. Plane atmosphere versus Spherical atmosphere. Ratio (A) and relative error (B) and absolute error (C) on transmittance T, for 5 scale factors and 2 optical depths $\tau = 0.1$ (i.e., $T = 0.9$) and $\tau = 1$ (i.e., $T = 0.3$).

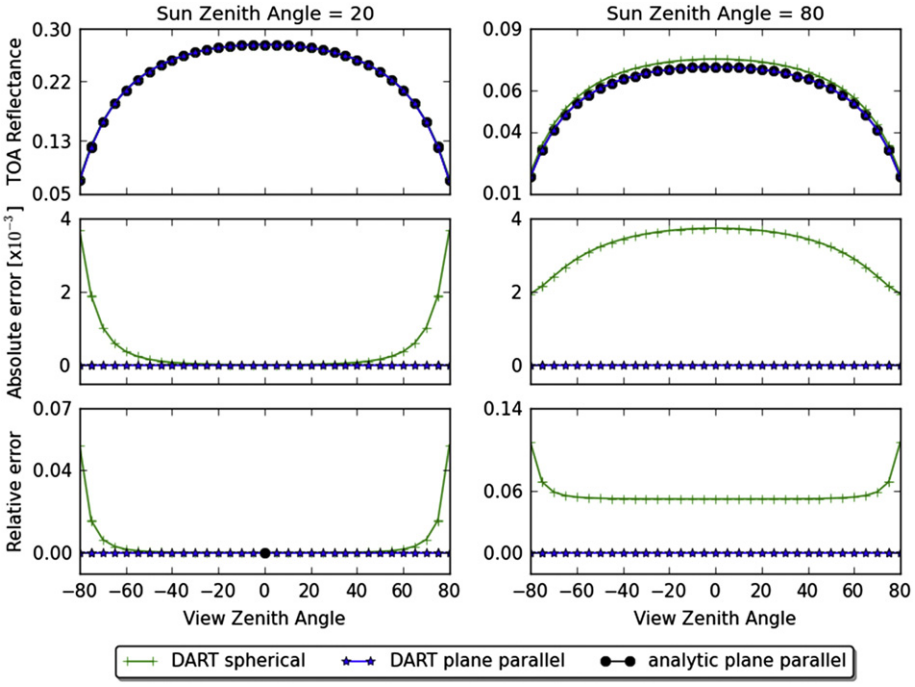

Fig. 16. TOA 1st order reflectance in the solar plane. DART with ($\rho^{DART}_{1,sphere,TOA}$) and without ($\rho^{DART}_{1,plane,TOA}$) account of Earth curvature (top) and associated absolute (middle) and relative (bottom) reflectance differences relative to analytic $\rho^{analytic}_{1,plane,TOA}$, for 2 sun off nadir angles (80°: left, 20°: right) and an absorbing atmosphere (transmittance = 0.75).

aimed to improve simulation accuracy while maintain acceptable computer times. For that, one introduced (1) transfer functions for transferring radiance values from one atmosphere level to another one, (2) an adaptation of Beer law, (3) mid-points M_s as origin of scattering for simulating exactly 1st order TOA and BOA radiance values, (4) an account of Earth curvature, and (5) an automatic computation of the atmosphere geometry. The major advantage of transfer functions is to decrease computer time in a very efficient way. Another advantage is that they can be computed for a specific atmosphere and applied to any landscape with the same atmosphere. This is very useful for operational work. The constraint of transfer functions is that the atmosphere is supposed to be horizontally homogeneous at any level z. Work is planned in order to circumvent this constraint in order to allow DART to consider clouds in the atmosphere, without excessively increasing computational time.

A number of numerical experiments were conducted for validating the new modeling approach. Comparison with theoretical expressions of atmosphere 1st order radiance proved the accuracy and reliability of the model for any optical thickness of the atmosphere and any angular configuration. The validity of the multiple scattering modeling was successfully tested with comparisons with MODTRAN simulations. As already mentioned, differences between DART and MODTRAN were always very small, even in the strong molecular scattering domains.

In short, the addition of an accurate atmospheric radiative transfer module to DART makes it an operational integrated model very efficient for remote sensing and radiative budget studies, in the UV, VIS, and IR domains. The new modeling of atmosphere radiative transfer is implemented in the DART model version 5.3.2 that is freely available for scientific work (http://www.cesbio.ups-tlse.fr/us/dart/dart_licence.html).

Acknowledgment

This work was supported by the Region Midi Pyrénées and by the Centre National d'Etudes Spatiales (CNES) in the frame of the project "High spatial resolution of the land surfaces with a geostationary satellite". The authors are also thankful to the team of scientists of the Space Center for Biosphere Studies (CESBIO) who contributes to the development of DART.

Appendix A. Within cell scattering

At first order (i.e., scattering of direct sun radiation), atmosphere layers scatter from a single point $M_s(\Omega_v)$ per scattering direction Ω_v. The altitude of $M_s(\Omega_v)$ is such that DART 1st order fluxes are exact in the case of an infinite plane atmosphere. At larger orders, multiple scattering is simulated from cell centers in order to decrease computer time. The computation of the altitude of $M_s(\Omega_v)$ is shown below.

The altitude of M_s in an air cell is driven by 2 factors that have opposite influences. This is shown here for a downward ray $W_{in}(z_i + \Delta z,\Omega_s)$ that crosses a layer i (Fig. 13) that is between the altitudes z_i and $z_i + \Delta z$ and the optical depths τ_i and $\tau_i + \Delta\tau$. $W_1(\Delta z/|\mu_s|,\Omega_s \rightarrow \Omega_v)$ is the within layer 1st order scattered flux along direction (Ω_v) and $W_{1,out}(z_i + \Delta z, \Omega_s \rightarrow \Omega_v)$ is the 1st order scattered flux that exits the layer.

Let us call E_s the TOA sun irradiance along direction (Ω_s) and $\tau(z)$ the atmosphere optical depth at the altitude z, with an origin at the top of the atmosphere (i.e., $\tau(\infty) = 0$ and $\tau(0) = \tau_o$). This layer has a gas optical depth $\Delta\tau_m$, an aerosol optical depth $\Delta\tau_p$ and a total optical depth $\Delta\tau = \Delta\tau_m + \Delta\tau_p$. Gasses have a total extinction coefficient α_m, a single scattering albedo ω_m and a phase function $P_m(\Omega_s,\Omega_v)$. Aerosols have a total extinction coefficient α_p, a single scattering albedo ω_p and a phase function $P_p(\Omega_s,\Omega_v)$.

For an atmosphere with extinction coefficient vertical profiles of gasses $\alpha_m(z)$ and aerosols $\alpha_p(z)$, with gas and aerosol height factors H_m and H_p, the layer mean extinction coefficients are:

$$\alpha_m = \frac{\tau_m\left[\exp\left(-\frac{z_i}{H_m}\right) - \exp\left(-\frac{z_i+\Delta z}{H_m}\right)\right]}{\Delta z}$$

$$\alpha_p = \frac{\tau_p\left[\exp\left(-\frac{z_i}{H_p}\right) - \exp\left(-\frac{z_i+\Delta z}{H_p}\right)\right]}{\Delta z}.$$

Let us call x the gas (m) or aerosol (p) components, $L^{exact}_{1,x}$ and $L^{DART}_{1,x}$ the layer exact and DART 1st order radiance, and $I^{DART}_{1,x}$ the DART 1st order intensity. The altitude of the scattering point $M_s(\Omega_v)$ (i.e., $z_i + \delta z'$ or $\tau_i + \delta\tau'$) must be such that we have: $L^{exact}_{1,x} =$

$L_{1,x}^{DART}$. The cases of upward ($\mu_v > 0$) and downward ($\mu_v < 0$) directions are analyzed below.

$\mu_v > 0$: Theory gives the exact upward 1st order radiance $L_{1,x}^{exact}(\Delta z,\Omega_v)$ scattered by component x. We have:

$$L_{1,x}^{exact}(\Delta z,\Omega_s,\Omega_v) = E_s(z_i+\Delta z)\cdot\omega_x\cdot\frac{P(\Omega_s,\Omega_v)}{4\pi}\cdot\int_{z_1+\Delta z}^{z_1}\times\exp\left[-\left(\alpha_m(z_i)+\alpha_p(z_i)\right)\cdot\left(\frac{1}{|\mu_s|}+\frac{1}{|\mu_v|}\right)\cdot(z_i+\Delta z-z)\right]\cdot\alpha_x(z_i)\cdot\frac{\Delta x\cdot\Delta y\cdot dz}{\Delta x\cdot\Delta y\cdot\mu_v}$$

$$\Rightarrow L_{1,x}^{exact}(\Delta z,\Omega_s,\Omega_v) = E_s(z_i+\Delta z)\cdot\omega_x\cdot\frac{P_x(\Omega_s,\Omega_v)}{4\pi}\cdot\frac{\alpha_x(z_i)}{\alpha_m(z_i)+\alpha_p(z_i)}\cdot\frac{|\mu_s|}{|\mu_s|+|\mu_v|}\cdot\left\{1-\exp\left(-\Delta\tau_i\cdot\frac{|\mu_s|+|\mu_v|}{|\mu_s|\cdot|\mu_v|}\right)\right\}.$$

Note. Total radiance is:

$$L^{exact}(\Delta z,\Omega_s,\Omega_v) = E_s(z_i+\Delta z).\omega.\frac{P(\Omega_s,\Omega_v)}{4\pi}\frac{|\mu_s|}{|\mu_s|+|\mu_v|}.\left\{1-\exp\left(-\Delta\tau_i.\frac{|\mu_s|+|\mu_v|}{|\mu_s|.|\mu_v|}\right)\right\}.$$

With $\omega.\frac{P(\Omega_s,\Omega_v)}{4\pi} = \left[\alpha_m(z_i).\omega_m.\frac{P_m(\Omega_s,\Omega_v)}{4\pi}+\alpha_p(z_i).\omega_p.\frac{P_p(\Omega_s,\Omega_v)}{4\pi}\right]\cdot\frac{1}{\alpha_m(z_i)+\alpha_p(z_i)}$

DART 1st order intensity is: $I_{1,x}^{DART}(\Delta z,\Omega_s,\Omega_v) = \omega_x.\frac{P_x(\Omega_s,\Omega_v)}{4\pi}.W_{int,x}.\exp\left[-\frac{\delta\tau_x'}{|\mu_v|}\right]$ with x interception:

$$W_{int,x} = E_s(z_i+\Delta z).\int_{z_i+\Delta z}^{z_i}\exp\left[-\left(\alpha_m(z_i)+\alpha_p(z_i)\right).(z_i+\Delta z-z)\right].\alpha_x(z_i).\Delta x.\Delta y.dz$$

$$W_{int,x} = E_s(z_i+\Delta z)\frac{\alpha_x(z_i)}{\alpha_m(z_i)+\alpha_p(z_i)}.|\mu_s|.\left\{1-\exp\left(-\frac{\Delta\tau_i}{|\mu_s|}\right)\right\}.\Delta x.\Delta y.$$

Thus, DART 1st order radiance for component x is:

$$L_{1,x}^{DART}(\Delta z,\Omega_s,\Omega_v) = \frac{L_{1,x}^{DART}(\Delta z,\Omega_s,\Omega_v)}{\Delta x\cdot\Delta y\cdot|\mu_v|} = E_s(z_i+\Delta z)\cdot\omega_x\cdot\frac{P_x(\Omega_s,\Omega_v)}{4\pi}\cdot\frac{\alpha_x(z_i)}{\alpha_m(z_i)+\alpha_p(z_i)}\cdot\left\{1-\exp\left(-\frac{\Delta\tau_i}{|\mu_s|}\right)\right\}\cdot\frac{|\mu_s|}{|\mu_v|}\cdot\exp\left[-\frac{\delta\tau_x'}{|\mu_v|}\right].$$

Condition "$L_{1,x}^{exact}(\Delta z,\Omega_s,\Omega_v) = L_{1,x}^{DART}(\Delta z,\Omega_s,\Omega_v)$" is verified if:

$$\delta\tau_x' = -|\mu_v|.\ln\left(\frac{|\mu_v|}{|\mu_s|+|\mu_v|}\cdot\frac{1-\exp\left[-\Delta\tau_i.\frac{|\mu_s|+|\mu_v|}{|\mu_s|.|\mu_v|}\right]}{1-\exp\left[-\frac{\Delta\tau_i}{|\mu_s|}\right]}\right).$$

It appears that $\delta\tau_x'$ does not depend specifically on $\Delta\tau_x$. Thus, we have:

$$\delta\tau_m' = \delta\tau_p' = \delta\tau' = -|\mu_v|.\ln\left(\frac{|\mu_v|}{|\mu_s|+|\mu_v|}\cdot\frac{1-\exp\left[-\Delta\tau_i.\frac{|\mu_s|+|\mu_v|}{|\mu_s|.|\mu_v|}\right]}{1-\exp\left[-\frac{\Delta\tau_i}{|\mu_s|}\right]}\right)\text{ and }\delta z' = \frac{\delta\tau'}{\alpha_m(z_i)+\alpha_p(z_i)}.$$

The validity of the expression of $\delta\tau'$ can be verified with a Taylor expansion, for the case $\Delta\tau \ll 1$:

$$\frac{|\mu_v|}{|\mu_s|+|\mu_v|}\cdot\frac{1-\exp\left[-\Delta\tau_i.\frac{|\mu_s|+|\mu_v|}{|\mu_s|.|\mu_v|}\right]}{1-\exp\left[-\frac{\Delta\tau_i}{|\mu_s|}\right]}\approx 1+\frac{B-A}{2}\Delta\tau_i+\left(\frac{A^2}{6}-\frac{A.B}{4}+\frac{B^2}{12}\right).\Delta\tau_i^2+\ldots$$

with $A = \frac{|\mu_s|+|\mu_v|}{|\mu_s|.|\mu_v|}$ and $B = \frac{1}{|\mu_s|}$

$$\Rightarrow\delta\tau'\approx\frac{A-B}{2}.\mu_v.\Delta\tau_i+\frac{B^2-A^2}{24}.\mu_v.\Delta\tau_i^2+\ldots$$
$$\Rightarrow\delta\tau'\approx\frac{\Delta\tau_i}{2}-\left(\frac{1}{|\mu_v|}+\frac{2}{|\mu_s|}\right).\frac{\Delta\tau_i^2}{24}.$$

It means that for small $\Delta\tau_i$ values, the origin point for scattering is located above the cell center. It is all the more above the cell center that the illumination and scattering directions are oblique. If $\Delta\tau_i = 0.1$, the ratio $\frac{\delta\tau'-\Delta\tau_i}{\Delta\tau_i}$ is around 5%, if incident and scattering directions have a zenith angle equal to 60°. In that case, the relative error on transmittance is $\approx 5\ 10^{-3}$.

$\mu_v < 0 \neq \mu_s$: Theory gives the exact upward 1st order radiance $L_{1,x}^{exact}(\Delta z,\Omega_v)$ scattered by component x. We have:

$$L_{1,x}^{exact}(\Delta z,\Omega_s,\Omega_v) = E_s(z_i+\Delta z).\omega_x.\frac{P(\Omega_s,\Omega_v)}{4\pi}.\int_{z_1+\Delta z}^{z_1}\times\exp\left[-\left(\alpha_m(z_i)+\alpha_p(z_i)\right).\left(\frac{z_i+\Delta z-z}{|\mu_s|}+\frac{z-z_i}{|\mu_v|}\right)\right].\alpha_x(z_i).\frac{\Delta x.\Delta y.dz}{\Delta x.\Delta y.\mu_v}$$

$$\Rightarrow L_{1,x}^{exact}(\Delta z,\Omega_s,\Omega_v) = E_s(z_i+\Delta z).\omega_x\frac{Px(\Omega_s,\Omega_v)}{4\pi}.\frac{\alpha_x(z_i)}{\alpha_m(z_i)+\alpha_p(z_i)}.\frac{|\mu_s|}{|\mu_s|-|\mu_v|}.\left\{\exp\left(-\frac{\Delta\tau_i}{|\mu_s|}\right)-\exp\left(-\frac{\Delta\tau_i}{|\mu_v|}\right)\right\}.$$

DART 1st order radiance for component x is:

$$L_{1,x}^{exact}(\Delta z,\Omega_s,\Omega_v) = E_s(z_i+\Delta z).\omega_x\frac{P_x(\Omega_s,\Omega_v)}{4\pi}.\frac{\alpha_x(z_i)}{\alpha_m(z_i)+\alpha_p(z_i)}.\left\{1-\exp\left(-\frac{\Delta\tau_i}{|\mu_s|}\right)\right\}\frac{|\mu_s|}{|\mu_v|}.\exp\left[-\frac{\Delta\tau_i}{|\mu_v|}\right].\exp-\frac{\delta\tau_x'}{|\mu_v|}.$$

Condition "$L_{1,x}^{exact}(\Delta z,\Omega_s,\Omega_v) = L_{1,x}^{DART}(\Delta z,\Omega_s,\Omega_v)$" is verified if:

$$\delta\tau_x' = \mu_v.\ln\left(\frac{|\mu_v|}{|\mu_v|-|\mu_s|}\cdot\frac{1-\exp\left[-\Delta\tau_i.\frac{|\mu_v|-|\mu_s|}{|\mu_s|.|\mu_v|}\right]}{1-\exp\left[-\frac{\Delta\tau_i}{|\mu_s|}\right]}\right).$$

Because $\delta\tau_x'$ does not depend specifically on $\Delta\tau_x$, we have:

$$\delta\tau_m' = \delta\tau_p' = \delta\tau' = \mu_v.\ln\left(\frac{|\mu_v|}{|\mu_v|-|\mu_s|}\cdot\frac{1-\exp\left[-\Delta\tau_i.\frac{|\mu_v|-|\mu_s|}{|\mu_s|.|\mu_v|}\right]}{1-\exp\left[-\frac{\Delta\tau_i}{|\mu_s|}\right]}\right)\text{ and }\delta z' = \frac{\delta\tau'}{\alpha_m(z_i)+\alpha_p(z_i)}.$$

The validity of the expression of $\delta\tau'$ can be verified with a Taylor expansion, for the case $\Delta\tau \ll 1$:

$$\frac{|\mu_v|}{|\mu_v|-|\mu_s|}.\frac{1-\exp\left[-\Delta\tau_i.\frac{|\mu_v|-|\mu_s|}{|\mu_s|.|\mu_v|}\right]}{1-\exp\left[-\frac{\Delta\tau_i}{|\mu_s|}\right]} \approx 1+\frac{B-A}{2}\Delta\tau_i + \left(\frac{A^2}{6}-\frac{A.B}{4}+\frac{B^2}{12}\right).\Delta\tau_i^2+\ldots$$

with $A=\frac{|\mu_v|-|\mu_s|}{|\mu_s|.|\mu_v|}$ and $B=\frac{1}{|\mu_s|}$

$$\Rightarrow \delta\tau' \approx \frac{B-A}{2}.|\mu_v|.\Delta\tau_i+\frac{A^2-B^2}{24}.|\mu_v|.\Delta\tau_i^2+\ldots$$
$$\Rightarrow \delta\tau' \approx \frac{\Delta\tau_i}{2}-\left(\frac{1}{|\mu_v|}-\frac{2}{|\mu_s|}\right).\frac{\Delta\tau_i^2}{24}.$$

It means that for small $\Delta\tau_i$, the origin point for scattering is above the cell center if the illumination direction is much more oblique than the scattering direction (e.g., $|\mu_s| < 2|\mu_v|$).

$\boldsymbol{\mu_v = \mu_s < 0}$: $L_{1,x}^{exact}(\Delta z,\Omega_s,\Omega_v) = E_s(z_i+\Delta z).\omega_x.\frac{P_x(\Omega_s,\Omega_v)}{4\pi}.\frac{\alpha_x(z_i)}{\alpha_m(z_i)+\alpha_p(z_i)} .\frac{\Delta\tau_i}{|\mu_s|}.\exp\left(-\frac{\Delta\tau_i}{|\mu_s|}\right)$.

$$L_{1,x}^{exact}(\Delta z,\Omega_s,\Omega_v) = E_s(z_i+\Delta z).\omega_x.\frac{P(\Omega_s,\Omega_v)}{4\pi}.\frac{\alpha_x(z_i)}{\alpha_m(z_i)+\alpha_p(z_i)} .\left\{1-\exp\left(-\frac{\Delta\tau_i}{|\mu_s|}\right)\right\}.\exp\left[-\frac{\Delta\tau_i}{|\mu_s|}\right].\exp\left[\frac{\delta\tau_x'}{|\mu_s|}\right]$$

$$L_{1,x}^{exact}(\Delta z,\Omega_s,\Omega_v) = L_{1,x}^{DART}(\Delta z,\Omega_s,\Omega_v) \Rightarrow \delta\tau' = |\mu_s|.\ln\left(\frac{\Delta\tau_i}{|\mu_v|}.\frac{1}{1-\exp\left[-\frac{\Delta\tau_i}{|\mu_v|}\right]}\right)$$

In short, the above expressions stress that optical depth $\delta\tau'$ depends on the view direction (Ω_v) and that $\delta\tau'_m = \delta\tau'_p$. For very small $\Delta\tau_i$ (i.e., very small layer gas and aerosol densities), Taylor expansions show that M_s is very close to the cell center (i.e., $\Delta\tau_i' \approx \frac{\Delta\tau_i}{2}$). However, to simulate the atmosphere as the superimposition of layers with very small optical depths would require a very large number of layers that cannot be managed in the R.T. model such as DART. This justifies the use of points M_s for 1st order scattering.

It is interesting to note that within cell multiple scattering is simulated in a different way as in vegetation cells. An air cell intercepts part of its own 1st scattering order radiation, which leads to within cell multiple scattering. Conversely to vegetation cells, within cell multiple scattering is not simulated at the same stage as 1st scattering order radiation. It is simulated at the following stage with incident radiation that comes from other cells and that is intercepted by this cell. However, similarly to vegetation cells, multiple scattering is simulated using intercepted radiation that is stored per incident direction on the cell, separately for gasses and molecules, to take into account their different phase functions.

Section 4 presents how DART reflectance is improved due to the use of mid-points M_s.

Points M_s are not used in DART mode T (i.e., thermal emission). Atmosphere thermal emission is computed per layer with the altitude dependent extinction coefficients

$$\alpha_{abs}(\lambda) = \alpha_{abs}^m(\lambda)+\alpha_{abs}^p(\lambda) \quad \text{and} \quad \alpha_{scat}(\lambda) = \alpha_{scat}^m(\lambda)+\alpha_{scat}^p(\lambda).$$

Total extinction coefficient is: $\alpha_e(z,\lambda) = \alpha_{abs}(z,\lambda) + \alpha_{scat}(z,\lambda)$ with single scattering albedo

$$\omega^m(z,\lambda) = \frac{\alpha_{scat}^m(z,\lambda)}{\alpha_{scat}^m(\lambda)+\alpha_{abs}^m(\lambda)} \quad \text{and} \quad \omega^p(z,\lambda) = \frac{\alpha_{scat}^p(z,\lambda)}{\alpha_{scat}^p(\lambda)+\alpha_{abs}^p(\lambda)}.$$

A cell gives rise to a unique ray along a given direction, with an origin that is located on the top or bottom cell face, depending if the ray direction is upward or downward. The vector source W_A emitted along (Ω, $\Delta\Omega$) is due to the emission of an oblique parallelepiped (height Δz, base $\Delta x.\Delta y$):

$$W_A(\lambda,T) = \Delta x\cdot\Delta y\cdot\alpha_{abs}(\lambda)\cdot L_B(\lambda,T)\cdot\Delta\Omega\cdot\int_0^{\Delta z}\exp\left[-\alpha_e(z,\lambda)\cdot\frac{z}{\cos(\theta)}\right]\cdot dz \qquad \left[W\cdot\mu m^{-1}\right]$$

$$W_A(\lambda,T) = \varepsilon(\lambda)\cdot L_B(\lambda,T)\cdot\Delta x\cdot\Delta y\cdot\cos\theta\cdot\left[1-\exp\left(-\alpha_e(z,\lambda)\cdot\frac{\Delta z}{\cos(\theta)}\right)\right]\cdot\Delta\Omega = L_A(\lambda,T)\cdot S_{eff}\cdot\Delta\Omega$$

where $S_{eff} = \Delta x.\Delta y.\cos\theta$, $\varepsilon(\lambda) = \frac{\alpha_a(\lambda)}{\alpha_e(\lambda)}$, and $L_A(\lambda,T)$ is the atmosphere radiance ($W.m^{-2}.sr^{-1}.\mu m^{-1}$).

Appendix B. Earth curvature

For very oblique sun and view directions (i.e., far from local vertical), the atmosphere should not be treated as a horizontal plane. Indeed, for an off-nadir angle θ, an atmosphere path length between altitudes z_A and z_B is smaller than in a horizontal atmosphere (i.e., $\Delta z/|\mu|$, with $\mu = \cos\theta$ and $\Delta z = |z_A - z_B|$). This difference of path lengths must be analyzed in conjunction with the fact that gas and aerosol vertical densities are not constant. DART R.T. modeling considers the Earth curvature. For that the "Atmosphere–Earth" system is assumed to be a sphere. The adopted approach is presented below.

Fig. 14 shows a path AB along a direction with a θ zenith angle in a spherical atmosphere. R_T is the Earth radius and R(z) the radius of the sphere at the altitude z. Thus, for point A, we have: $R_A(z) = R_T + z$. Hereafter, we consider an upward path (i.e., $\mu = \cos(\theta) > 0$) and a downward path (i.e., $\mu = \cos(\theta) < 0$).

$\mu > 0$: Path $\{\Delta z > 0; \mu\}$ is $AB = -R_A.\mu + \sqrt{R_A^2.\mu^2 + \Delta z.(\Delta z + 2R_A)}$. It can be treated as a path $\{\Delta z; \mu_{sph}\}$ in an horizontal atmosphere if we replace μ by $\mu_{sph} = \frac{\Delta z}{-R_A.\mu+\sqrt{R_A^2.\mu^2+\Delta z.(\Delta z+2R_A)}}$.

Then $AB = \frac{\Delta z}{\mu_{sph}} < \frac{\Delta z}{\mu}$.

$\mu < 0$: Path $\{\Delta z < 0; \mu\}$ is $AB = -R_A.\mu - \sqrt{R_A^2.\mu^2 + \Delta z.(\Delta z - 2R_A)}$. It can be treated as a path $\{\Delta z; \mu_{sph}\}$ in a horizontal atmosphere if we replace μ by $\mu_{sph} = \frac{-\Delta z}{R_A.\mu+\sqrt{R_A^2.\mu^2+\Delta z.(\Delta z-2R_A)}}$.

Then: $AB = \frac{-\Delta z}{\mu_{sph}} < \frac{-\Delta z}{\mu}$.

The 2 expressions of AB and μ_{sph} are identical. Indeed: $\{\mu > 0, \Delta z > 0\}$ for the 1st one and $\{\mu < 0, \Delta z < 0\}$ for the 2nd one. As expected, they stress that a path between 2 altitude levels is smaller in a spherical atmosphere than in a horizontal atmosphere.

The optical depth of path AB is:

$$\Delta\tau(z_A,\Delta z,\mu) = \int_0^{\Delta l=AB}\alpha(t)\cdot dl = \int_{z_A}^{z_B}\alpha(t).\frac{R_A+t}{\sqrt{R_A^2.\mu^2+t.(t+2R_A)}}\cdot dt$$

with t the altitude relative to z_A and l the path length starting from A:

$$\mu>0: \quad l = -R_A \cdot \mu + \sqrt{R_A^2 \cdot \mu^2 + t \cdot (t + 2R_A)}$$
$$\mu<0: \quad l = -R_A \cdot \mu - \sqrt{R_A^2 \cdot \mu^2 + t \cdot (t - 2R_A)}.$$

Let us consider the x component (m: gas; p: aerosol) and a layer i [z_i $z_i + \Delta z_i$] of a plane atmosphere with a mean extinction coefficient $\overline{\alpha_i}$. DART optical depth of a path Δl_{plane} along a direction μ_j with a vertical variation Δz is: $\Delta\tau_{plane,x}\left(z, \Delta z, \mu_j\right) = \overline{\alpha_{x,i}}(z) \cdot \Delta l_{plane} = \overline{\alpha_{x,i}}(z) \cdot \left|\frac{\Delta z}{\mu_j}\right|$.

In order to keep the rectangular geometry of DART scenes, the spherical atmosphere is treated as a horizontal atmosphere. For that, in the classical R.T. equations for a plane atmosphere, the term μ_j is replaced by the term $\mu_{sph,x,i,j}$ that is defined by: $\Delta\tau_{sph,x}\left(z, \Delta z, \mu_j\right) = \overline{\alpha_{x,i}}(z).\left|\frac{\Delta z}{\mu_{sph,x,i,j}}\right|$.

Any DART atmosphere layer is usually too thick in order to consider that $\alpha_x(z)$ is constant within it to compute the effect of earth curvature. Thus, the optical depth is computed with the integral:

$$\Delta\tau_{sph,x}\left(z, \Delta z, \mu_j\right) = \int_z^{z+\Delta z} \alpha_x(t) \cdot F(t) \cdot dt \quad \text{with} \quad F(t) = \frac{R_T + t}{\sqrt{R_T^2 \cdot \mu^2 + t \cdot (t + 2R_T)}}.$$

For practical reasons, when the atmosphere R.T. is running, parameter $\alpha_x(z)$ is not reachable, conversely to the i discrete extinction coefficients $\overline{\alpha_{x,i}}$ and the total optical depth τ_x. Because $\alpha_x(z)$ is not fully defined by $\overline{\alpha_{x,i}}$, component x in any layer i is assumed to have an exponential distribution with the same height factor H_x in all layers (e.g., $H_m = 8$ km, $H_p = 2$ km). Thus, in any layer i, we have $\alpha_{x,i,\lambda} = \alpha_{x,0,i} \cdot \exp\left(-\frac{z}{H_x}\right)$, where $\alpha_{o,i}$ is the extinction coefficient at altitude $z = 0$. It must be noted that this approach works with any vertical distribution of atmospheric constituents, even for components with non-vertical distribution.

For each layer i, one has:

$$\overline{\alpha_{x,i}} = \frac{1}{\Delta z_i}\int_{z_i}^{z_i+\Delta z_i} \alpha_x(z) \cdot dz = \frac{\alpha_{x,0,i}}{\Delta z_i}\int_{z_i}^{z_i+\Delta z_i} \exp\left(-\frac{z}{H_x}\right) \cdot dz = \frac{\alpha_{x,0,i}.H_x}{\Delta z_i}\left[\exp\left(-\frac{z_i}{H_x}\right) - \exp\left(-\frac{z_i + \Delta z_i}{H_x}\right)\right].$$

Thus, for each layer i, we have:

$$\alpha_{x,0,i} = \frac{\overline{\alpha_{x,i}} \cdot \Delta z_i}{H_x} \cdot \frac{1}{\exp\left(-\frac{z_i}{H_x}\right) - \exp\left(-\frac{z_i + \Delta z_i}{H_x}\right)}.$$

Finally, in order to verify the equality $\Delta\tau_{sph,x,i}\left(z_i, \Delta z_i, \mu_j\right) = \overline{\alpha_{x,i}} \cdot \left|\frac{\Delta z_i}{\mu_{sph,x,i,j}}\right|$, we must have:

$$\left|\mu_{sph,x,i,j}\right| = \frac{\overline{\alpha_{x,i}}(z)}{\Delta\tau_{sph,x,i}\left(z_i, \Delta z_i, \mu_j\right)} .\Delta z_i$$

$|\mu_{sph,x,i,j}|$ is computed for the 2 components (i.e., aerosols and gasses), the N_{layers} atmosphere layers, the N_{dir} discrete directions and the N_λ spectral bands.

Fig. 15 illustrates the impact of the Earth curvature on the gas atmosphere transmittance, for 5 atmosphere scale factors and 2 optical depths $\tau = 0.1$ (i.e., $T = 0.9$) and $\tau = 1$ (i.e., $T = 0.37$). As expected, the ratio $\frac{\mu_{plane}}{\mu_{sph}}$ and the relative and absolute errors on atmosphere transmittance vary as a function of zenith angle θ (Fig. 15a), especially for $\theta > 50°$. For an atmosphere with an optical depth $\Delta\tau_{atm}$ equal to 0.1, the relative error on atmosphere direct transmittance reaches 25% for an 85° zenith angle. We verify also that the relative error increases with zenith angles. The absolute error on atmosphere transmittance behaves differently, because transmittance tends to the 0 value for larger zenith angles: if $\Delta\tau_{atm}$ increases, the maximal absolute error on atmosphere transmittance arises for zenith angles smaller than 90°. For example, Fig. 15c shows that the maximal absolute error occurs for $\theta \approx 70°$ if $\tau = 1$.

The interest to consider the Earth curvature is shown here by comparing 3 computations of TOA atmosphere 1st order reflectance: DART simulation $\rho^{DART}_{1,sphere,TOA}$ with the "Earth curvature" correction, DART simulation $\rho^{DART}_{1,plane,TOA}$ for a plane atmosphere and an analytically computed reflectance $\rho^{analytic}_{1,plane,TOA}$ for a plane atmosphere. Here, we consider a pure absorbing atmosphere with nadir transmittance T_{abs}, an Earth surface with a Lambertian reflectance ρ_{ground}, a sun direction Ω_s and a view direction Ω_v. Then:

$$\rho^{analytic}_{1,plane,TOA}(\Omega_s, \Omega_v) = \rho_{ground}.T_{abs}^{\left(\frac{1}{|\mu_s|} + \frac{1}{|\mu_v|}\right)} \quad \text{with } \mu_s = \cos(\theta_s) \text{ and } \mu_v = \cos(\theta_v).$$

Fig. 16 shows the reflectance values $\rho^{DART}_{1,sphere,TOA}$, $\rho^{DART}_{1,plane,TOA}$ and $\rho_{1,plane,TOA}{}^{analytic}$ and their associated absolute and relative differences, for 2 off-nadir sun directions θ_s (i.e., 20° and 80°), with a Lambertian Earth surface ($\rho_{ground} = 0.5$). As expected, DART reflectance $\rho_{1,plane,TOA}{}^{DART}$ that is simulated with no account of the Earth curvature is equal to the analytic reflectance $\rho^{analytic}_{1,plane,TOA}$ for a plane atmosphere. Indeed, the DART simulated atmosphere transmittance is equal to the one used by the analytic reflectance. On the other hand, differences occur with $\rho^{DART}_{1,sphere,TOA}$, due to the account of the Earth curvature. Differences are all larger than sun and/or view directions are oblique. For $\theta_s = 20°$, relative differences are almost zero for $\theta_v < 60°$, and reach 5% for $\theta_v = 80°$. Relative difference is much larger for $\theta_s = 80°$: it is ≈6% (i.e., absolute difference ≈ 0.0035) for a nadir view direction $\theta_v = 0°$. The absolute difference decreases with larger θ_v, similarly to the decrease of TOA reflectance. However, relative differences remain at ≈6% level for $\theta_v < 60°$. For $\theta_v > 60°$, relative differences increase strongly. These results confirm the interest to take into account the Earth curvature when modeling R.T., especially for far-off nadir sun and view directions.

References

Adams, C. N., & Kattawar, G. W. (1970). Solutions of the equation of radiative transfer by an invariant imbedding approach. *J. Quant. Spectrosc. Radiat. Transfer, 10*, 341–366.

Barbier, N., Couteron, P., Proisy, C., Yadvinder, M., & Gastellu-Etchegorry, J. -P. (2010). The variation of apparent crown size and canopy heterogeneity across lowland Amazonian forests. *Global Ecology and Biogeography*, http://dx.doi.org/10.1111/j.1466-8238.2009.00493.

Belot, A. (2007). *Simulation des échanges d'énergie et de masse d'un couvert végétal: Développement et validation d'un modèle quasi 3D, DART-EB. PhD.* http://www.cesbio.ups-tlse.fr/us/these_list.htm. Agro Paris Tech

Berk, A., & Bernstein (1989). *MODTRAN: A moderate resolution model for LOWTRAN 7.* final report. Bedford Geophysics Lab.

Berk, A., & Bernstein (1999). *MODTRAN4 radiative transfer modeling for atmospheric correction., Vol. 3756.* (pp. 348–353).

Bird, R. E., & Riordan, C. (1984). Simple solar spectral model for direct and diffuse irradiance on horizontal and tilted planes at the Earth's surface for cloudless atmospheres. *Technical report no. SERI/TR-215-2436.* Golden, CO: Solar Energy Research Institute.

Bulcholtz, A. (1995). Rayleigh scattering calculations for terrestrial atmosphere. *Applied Optics, 34*, 2765–2773.

Chandrasekhar, S. (1960). *Radiative transfer.* New York: Dover, 49 (Chap. 1).

Chetwynd, J. G., Wang, J., & Anderson, G. P. (1994). FASCODE: An update and applications in atmospheric remote sensing. *Proceedings of SPIE, 2266.*

Clough, S. A., Shephard, M. W., Mlawer, E. J., Delamere, J. S., Iacono, M. J., Cady-Pereira, K., et al. (2005). Atmospheric radiative transfer modeling: A summary of the AER codes. *Journal of Quantitative Spectroscopy and Radiation Transfer, 91*, 233–244.

Couturier, S., Gastellu-Etchegorry, J. P., Patiño, P., & Martin, E. (2009). A model-based performance test for forest classifiers on remote sensing imagery. *Forest Ecology and Management, 257*(1), 23–37.

Dave, J. V. (1980). Effect of atmospheric conditions on remote sensing of a surface nonhomogeneity. *Photogrammetric Engineering and Remote Sensing, 46*(9), 1173–1180.

Deutschmann, T., Beirle, S., Friess, U., Grzegorski, M., Kern, C., Kritten, L., et al. (2011). The Monte Carlo atmospheric radiative transfer model McArtim: Introduction and validation of Jacobians and 3D features. *Journal of Quantitative Spectroscopy and Radiative Transfer*, *112*(6), 1119–1137.

Drayson, S. R. (1976). Rapid computation of Voigt profile. *Journal of Quantitative Spectroscopy and Radiative Transfer*, *16*(7), 611–614.

Duthoit, S., Demarez, V., Gastellu-Etchegorry, J. P., Martin, E., & Roujean, J. L. (2008). Assessing the effects of the clumping phenomenon on BRDF and fAPAR of a maize crop based on 3D numerical scenes using DART code. *Agricultural and Forest Meteorology*, *1341–1352*.

Edwards, D. P. (1992). *GENLN2: A general line-by-line atmospheric transmittance and radiance model, Version 3.0 description and users guide.* NCAR/TN-367-STR. Boulder, Co: National Center for Atmospheric Research.

Evans, K. F. (1998). The spherical harmonic discrete ordinate method for three-dimensional atmospheric radiative transfer. *Journal of the Atmospheric Sciences*, *55*, 429–446.

Eymet, V., Fournier, R., Blanco, S., & Dufresne, J. -L. (2004). A boundary-based net-exchange Monte-Carlo method for absorbing and scattering thick media. *Journal of Quantitative Spectroscopy and Radiation Transfer*, *95*, 27–46.

Fu, Q., & Liou, K. (1993). Parametrization of the radiative properties of cirrus clouds. *Journal of the Atmospheric Sciences*, *50*, 2008–2025.

Garcia, R. D.M., & Siewert, C. E. (1989). The FN method for radiative transfer models that include polarization effects. *Journal of Quantitative Spectroscopy and Radiation Transfer*, *41*, 117–145.

Gascon, F. (2001). Modélisation physique d'images de télédétection optique. (PhD). http://www.cesbio.ups-tlse.fr/us/these_list.htm

Gastellu-Etchegorry, J. P. (2008). 3D modeling of satellite spectral images—Radiation budget and energy budget of urban landscapes. *Meteorology and Atmosphere Physics*, *102*(3–4), 187–207.

Gastellu-Etchegorry, J. P., & Zagolski, F. (1996). A simple anisotropic reflectance model for homogeneous multi-layer canopies. *Remote Sensing of Environment*, *57*, 22–38.

Gordley, L. L., Marshall, B. T., & Chu, A. (1994). LINEPAK: Algorithm for modeling spectral transmittance and radiance. *Journal of Quantitative Spectroscopy and Radiation Transfer*, *52*(5), 563–580.

Guillevic, P., Gastellu-Etchegorry, J. P., Demarty, J., & Prévot, L. (2003). Thermal infrared radiative transfer within three-dimensional vegetation cover. *Journal of Geophysical Research—Atmosphere*, *108*(D8), http://dx.doi.org/10.1029/2002JD002247.

Hansen, J. E. (1971). Multiple scattering of polarized light in planetary atmospheres. Part II. Sunlight reflected by terrestrial water clouds. *Journal of the Atmospheric Sciences*, *28*, 1400–1426.

Hay, J. E., & Davies, J. A. (1978). Calculation of the solar radiation: Incident on an inclined surface. In J. E. Hay, & T. K. Won (Eds.), *Proc. First Canadian Solar Data Workshop* Toronto, Canada.

Lee, T. Y., & Kaufman, Y. J. (1986). Non-lambertian effects on remote sensing of surface reflectance and vegetation index. *IEEE Transactions on Geoscience and Remote Sensing*, *24*(5), 699–708.

Key, J., & Schweiger, A. J. (1998). Tools for atmospheric radiative transfer: Streamer and FluxNet. *Computers & Geosciences*, *24*(5), 443–451.

Laurent, V. C. E., Verhoef, W., Clevers, J. G. P. W., & Schaepman, M. E. (2011). Estimating forest variables from top of-atmosphere radiance satellite measurements using coupled radiative transfer models. *Remote Sensing of Environment*, *115*, 1043–1052.

Lenoble, J., Herman, M., Deuze, J. L., Lafrance, B., Santer, R., & Tanré, D. (2007). A successive order of scattering code for solving the vector equation of transfer in the earth's atmosphere with aerosols. *Journal of Quantitative Spectroscopy and Radiation Transfer*, *107*, 479–507.

Lyapustin, A. I. (2005). Radiative transfer code SHARM for atmospheric and terrestrial applications. *Applied Optics*, *44*, 7764–7772.

Malenovsky, Z., Martin, E., Homolová, L., Gastellu-Etchegorry, J. P., Zurita-Milla, R., Schaepman, M. E., et al. (2008). Influence of woody elements of a Norway spruce canopy on nadir reflectance simulated by the DART model at very high spatial resolution. *Remote Sensing of Environment*, *112*, 1–18.

Marshall, B. T., & Gordley, L. L. (1994). BANDPAK: Algorithms for modeling broadband transmission and radiance. *Journal of Quantitative Spectroscopy and Radiation Transfer*, *52*(5), 581–599.

Martin, E. (2006). *DART Modèle 3D Multispectral et Inversion d'Images Optiques de Satellite - Application aux couverts forestiers.* (PhD). : Paul Sabatier University - Université de Toulouse (http://www.cesbio.ups-tlse.fr/us/these_list.htm).

Mayer, B., & Kylling, A. (2005). Technical note: The libRadtran software package for radiative transfer calculations—Description and examples of use. *Atmos. Chem. Phys.*, *5*, 1855–1877.

Mekler, Y., & Kaufman, Y. J. (1982). Contrast reduction by atmosphere and retrieval of nonuniform surface reflectance. *Applied Optics*, *21*(2), 310–316.

Mlawer, E. J., Taubman, S. J., Brown, P. D., Iacono, M. J., & Claugh, S. A. (1997). RRTM, a validated correlated-k model for the longwave. *Journal of Geophysical Research*, *102*(16), 663–682.

Plass, G. N., Kattawar, G. W., & Catchings, F. E. (1973). Matrix operator theory of radiative transfer. 1: Rayleigh-scattering. *Applied Optics*, *12*, 314–329.

Ricchiazzi, P., Yang, S. R., Gautier, C., & Sowle, D. (1998). SBDART: A research and teaching software tool for plane-parallel radiative transfer in the Earth's atmosphere. *Bulletin of the American meteorological soc*, *79*(10), 2101–2114.

Ross, J. (1981). *The radiation regime and architecture of plant stands.* The Hague: Dr Junk Publishers.

Rozanov, A., Rozanov, V., Buchwitz, M., Kokhanovsky, A., & Burrows, J. P. (2005). SCIATRAN 2.0—A new radiative transfer model for geophysical applications in the 175–2400 nm spectral region. *Advances in Space Research*, *36*(5), 1015–1019 (doi:10.1016).

Scott, N. A., & Chedin (1981). A fast line-by-line method for atmospheric absorption computations: The Automatized Atmospheric Absorption Atlas. *Journal of Applied Meteorology*, *20*, 802–812.

Sepulcre-Cantó, G., Zarco-Tejada, P. J., Sobrino, J. A., Berni, J. A. J., Jiménez Muñoz, J. C., & Gastellu-Etchegorry, J. P. (2009). Discriminating irrigated and rainfed olive orchards with thermal ASTER imagery and DART 3D simulation. *Agricultural and Forest Meteorology*, *149*, 962–975.

Sobrino, J., Mattar, C., Jiménez-Muñoza, J. C., Gastelllu-Etchegorry, J. P., & Grau, E. (2011). Evaluation of DART 3D model in the thermal domain using satellite/airborne imagery and ground-based measurements. *International Journal of Remote Sensing*, *32*(22), 7453–7477.

Stamnes, K., Tsay, S. -C., Wiscombe, W., & Laszlo, I. (2000). *DISORT, a general-purpose Fortran program for discrete-ordinate-method radiative transfer in scattering and emitting layered media: Documentation of methodology, tech. rep.* Hoboken, NJ: Dept. of Physics and Engineering Physics, Stevens Institute of Technology, 07030.

Timmermans, J. (2011). *Coupling optical and thermal directional radiative transfer to biophysical processes in vegetated canopies.* (PhD Thesis). : ITC, University of Twente (156pp., 978-90-6164).

Verhoef, W., & Bach, H. (2003). Simulation of hyperspectral and directional radiance images using coupled biophysical and atmospheric radiative transfer models. *Remote Sensing of Environment*, *87*, 23–41.

Verhoef, W., & Bach, H. (2007). Coupled soil-leaf-canopy and atmosphere radiative transfer modeling to simulate hyperspectral multi-angular surface reflectance and TOA radiance data. *Remote Sensing of Environment*, *109*, 166.

Vermote, E. F., Tanre, D., Deuze, J. L., Herman, M., & Morcrette, J. J. (1997). Second simulation of the satellite signal in the solar spectrum, 6S: An overview. *IEEE Transactions on Geoscience and Remote Sensing*, *35*(3), 675–686.

Widlowski, J. -L., Robustelli, M., Disney, M., Gastellu-Etchegorry, J. -P., Lavergne, T., Lewis, P., et al. (2008). The RAMI On-line Model Checker (ROMC): A web-based benchmarking facility for canopy reflectance models. *Remote Sensing of Environment*, *112*, 1144–1150.

Yin, T., Rubio, J., Grau, E., Lauret, N., Cros, J., & Gastellu-Etchegorry, J. P. (2012). *Direction discretization for radiative transfer modeling: An introduction to the new directional model of DART, IGARSS 2012, oral presentation.*

Young, A. T. (1980). Revised depolarization corrections for atmospheric extinction. *Applied Optics*, *19*, 3427–3428.

Zege, E. P., Katsev, I. L., & Polonsky, I. N. (1993). Multicomponent approach to light propagation in clouds and mists. *Applied Optics*, *32*, 2803–2812.

Zhai, P., Kattawar, G. W., & Yang, P. (2008). Impulse response solution to the three-dimensional vector radiative transfer equation in atmosphere-ocean systems. II. The hybrid matrix operator–Monte Carlo method. *Applied Optics*, *47*, 1063–1071.